

# Pervasive findings of directional selection realize the promise of ancient DNA to elucidate human adaptation

Ali Akbari<sup>1,2,3</sup>, Alison R. Barton<sup>2,3</sup>, Steven Gazal<sup>4,5,6</sup>, Zheng Li<sup>7</sup>, Mohammadreza Kariminejad<sup>8</sup>, Annabel Perry<sup>2,3</sup>, Yating Zeng<sup>4,9</sup>, Alissa Mittnik<sup>10</sup>, Nick Patterson<sup>2,3</sup>, Matthew Mah<sup>1,11</sup>, Xiang Zhou<sup>7</sup>, Alkes L. Price<sup>3,12,13</sup>, Eric S. Lander<sup>3,14,15</sup>, Ron Pinhasi<sup>16,17</sup>, Nadin Rohland<sup>1,2,3,11</sup>, Swapan Mallick<sup>1,2,3</sup>, and David Reich<sup>1,2,3,11</sup>

Correspondence to: [Ali\\_Akbari@hms.harvard.edu](mailto:Ali_Akbari@hms.harvard.edu), [reich@genetics.med.harvard.edu](mailto:reich@genetics.med.harvard.edu)

<sup>1</sup> Department of Genetics, Harvard Medical School, Boston, MA, USA

<sup>2</sup> Department of Human Evolutionary Biology, Harvard University, Cambridge, MA, USA

<sup>3</sup> Broad Institute of MIT and Harvard, Cambridge, MA, USA

<sup>4</sup> Department of Population and Public Health Sciences, Keck School of Medicine, University of Southern California, Los Angeles, CA, USA

<sup>5</sup> Center for Genetic Epidemiology, Keck School of Medicine, University of Southern California, Los Angeles, CA, USA

<sup>6</sup> Department of Quantitative and Computational Biology, University of Southern California, Los Angeles, CA, USA

<sup>7</sup> Department of Biostatistics, School of Public Health, University of Michigan, Ann Arbor, MI, USA

<sup>8</sup> Shamsipour Technical and Vocational College, Tehran, Iran

<sup>9</sup> Department of Biostatistics and Data Science, School of Public Health, The University of Texas Health Science Center at Houston, Houston, TX, USA

<sup>10</sup> Department of Archaeogenetics, Max Planck Institute for Evolutionary Anthropology, 04103 Leipzig, Germany

<sup>11</sup> Howard Hughes Medical Institute, Harvard Medical School, Boston, MA, USA

<sup>13</sup> Department of Epidemiology, Harvard T.H. Chan School of Public Health, Boston, MA, USA

<sup>14</sup> Department of Biostatistics, Harvard T.H. Chan School of Public Health, Boston, MA, USA

<sup>15</sup> Department of Systems Biology, Harvard Medical School, Boston, MA, USA

<sup>16</sup> Department of Biology, Massachusetts Institute of Technology (MIT), Cambridge, MA, USA

<sup>17</sup> Department of Evolutionary Anthropology, University of Vienna, Vienna, Austria

<sup>18</sup> Human Evolution and Archaeological Sciences, University of Vienna, Vienna, Austria

1 We present a method for detecting evidence of natural selection in ancient DNA time-  
2 series data that leverages an opportunity not utilized in previous scans: testing for a  
3 consistent trend in allele frequency change over time. By applying this to 8433 West  
4 Eurasians who lived over the past 14000 years and 6510 contemporary people, we find  
5 an order of magnitude more genome-wide significant signals than previous studies: 347  
6 independent loci with >99% probability of selection. Previous work showed that classic  
7 hard sweeps driving advantageous mutations to fixation have been rare over the broad  
8 span of human evolution, but in the last ten millennia, many hundreds of alleles have  
9 been affected by strong directional selection. Discoveries include an increase from ~0%  
10 to ~20% in 4000 years for the major risk factor for celiac disease at *HLA-DQB1*; a rise  
11 from ~0% to ~8% in 6000 years of blood type B; and fluctuating selection at the *TYK2*  
12 tuberculosis risk allele rising from ~2% to ~9% from ~5500 to ~3000 years ago before  
13 dropping to ~3%. We identify instances of coordinated selection on alleles affecting the  
14 same trait, with the polygenic score today predictive of body fat percentage decreasing  
15 by around a standard deviation over ten millennia, consistent with the “Thrifty Gene”  
16 hypothesis that a genetic predisposition to store energy during food scarcity became  
17 disadvantageous after farming. We also identify selection for combinations of alleles  
18 that are today associated with lighter skin color, lower risk for schizophrenia and  
19 bipolar disease, slower health decline, and increased measures related to cognitive  
20 performance (scores on intelligence tests, household income, and years of schooling).  
21 These traits are measured in modern industrialized societies, so what phenotypes were  
22 adaptive in the past is unclear. We estimate selection coefficients at 9.9 million variants,  
23 enabling study of how Darwinian forces couple to allelic effects and shape the genetic  
24 architecture of complex traits.  
25

26 Ancient DNA data hold extraordinary promise for revealing adaptation, making it possible to  
27 track effects across time and to obtain direct measurements of selection coefficients<sup>1–3</sup>.  
28 Rather than being trapped in the present and studying the scars left by selection on the  
29 genomes of descendants—for example, searching for alleles too differentiated in frequency  
30 across populations<sup>4,5</sup>, or too common given their estimated age<sup>6–8</sup>, or gene genealogies  
31 distorted from the expectation for random drift<sup>9</sup>—ancient DNA makes it possible to test if  
32 frequencies of variants shifted more than could be expected by chance. Such data also make it  
33 easier to measure selection on variants not of recent mutational origin, which is challenging  
34 to detect using retrospective methods<sup>10</sup>. Most previous ancient DNA selection studies focused  
35 on two time-points—comparing allele frequencies in earlier to later groups—to search for  
36 alleles with extreme shifts compared to expectation from the genomic background<sup>11,12</sup>. We  
37 search for a consistently non-zero derivative over time, fully embracing the time-series nature  
38 of ancient DNA and using information differently affected by confounding factors.  
39

40 Ancient DNA studies in West Eurasia<sup>11–14</sup> (Europe and its neighbors in the Near East) have  
41 identified dozens of alleles influenced by selection<sup>15,16</sup>. But despite growth in the number of  
42 ancient individuals with data from zero before 2010 to more than 10,000 today, the number  
43 of genome-wide significant loci reported in a single study grew only mildly: from 12 in the  
44 first genome scan in 2015<sup>11</sup>, to 21 in a scan in 2024<sup>14</sup>. The small numbers raise the concern  
45 that the power of ancient DNA to detect selection might be reaching a plateau, and that this  
46 approach might not in fact be able to deliver broad insights into the nature of adaptation.

47 **Three innovations increase statistical power and minimize false signals of selection**  
48 Our improved yield of discoveries comes from more power (due to a qualitatively new  
49 method and larger sample size), and fewer artifactual signals (due to intensive data cleaning).

50 First, we increased power by testing for a consistent trend in allele-frequency change over  
51 time. Most past studies of selection in ancient DNA dealt with the challenge posed by  
52 admixture by treating more recent populations as linear combinations of more ancient ones,  
53 then searching for alleles whose frequencies were outliers compared to what would be  
54 expected from this history. However, changes in frequency due to selection are often less  
55 than what can be expected from random genetic drift, and in this context, increasing sample  
56 size helps little. We employed a qualitatively different approach, using the genetic similarity  
57 of each individual to every other, and testing if the date when they lived provides additional  
58 predictive power for the allele frequencies of their population beyond what is expected from  
59 the empirical population structure. Our test is simple: at each variant we ask if hypothesizing  
60 a non-zero selection coefficient  $s$ —causing allele frequency to trend in the same direction  
61 over all times and places—predicts frequency differences across populations significantly  
62 better than empirically measured population structure alone (Methods).

63 Second, we increased power through a five-fold increase in sample size. We analyzed 8433  
64 unrelated ancient individuals from the last 14000 years<sup>17</sup> (Online Table 1). Data for 6686  
65 come from enriching ancient DNA libraries for more than a million single nucleotide  
66 polymorphisms (SNPs) where median coverage is 3.6-fold (at least 0.44-fold); the remaining  
67 1747 individuals are shotgun sequenced with median 1.6-fold coverage (at least 0.11-fold).  
68 For 3644 ancient individuals, sequences are previously reported. For 318, we increased data  
69 quality on previously reported individuals, largely from 300 newly reported shotgun genomes  
70 with median 4.9-fold coverage (40 at >17-fold coverage) (Online Table 2). For 4471 ancient  
71 individuals obtained by sequencing 5227 newly reported libraries (Online Table 3), we make  
72 data available for studies of selection with the support of sample custodians; archaeological  
73 contextual information will be provided in future publications which should be the references  
74 for analyses of their population history. We co-analyzed with 6510 modern people: 575  
75 largely from the 1000 Genomes Project<sup>18</sup>, and 5935 from the UK Biobank<sup>19</sup> (subsampled so  
76 their countries of origin were evenly spread over West Eurasia) (Extended Data Figure 1a,b).

77 Third, we increased power and reduced false positives by data cleaning and imputation. We  
78 applied multiple data quality filters, including restricting to sites with similar frequencies in  
79 ancestry-matched modern and ancient people and giving consistent signals of selection with  
80 and without modern people (Supplementary Information section 1). We filled in missing data  
81 by leveraging known patterns of allelic correlation, using GLIMPSE<sup>20</sup> to impute diploid  
82 genotypes and thereby increase allele counts at every locus (for imputation we used  
83 sequences aligning everywhere in the genome as we found that this greatly enhances  
84 information even for samples analyzed using in-solution enrichment). We analyzed 8,212,921  
85 SNPs and 1,713,563 insertions/deletions (indels) imputed at high quality across chromosomes  
86 1-22 in all individuals (we did not analyze the sex chromosomes or mitochondrial DNA).  
87

#### 88 A test for directional selection with a negligible false-positive rate

89 For each SNP in the genome, we estimate a selection coefficient, which we found has a  
90 standard error typically around 0.1% for common variants (Figure 2, Extended Data Figure  
91 1c). In theory, a valid test for selection should be  $Z$ , the number of standard errors this  
92 quantity is from zero, and we can use a normal distribution to identify scores that pass the  
93 standard threshold of genome-wide significance ( $P < 5 \times 10^{-8}$ ) for Genome-Wide Association  
94 Studies (GWAS). In practice, the median  $\chi^2$  statistic (squared  $Z$ -score for number of standard  
95 errors  $s$  is from zero) is inflated by 5.26-fold relative to a  $\chi^2$  distribution with one degree of  
96 freedom. In human genetics studies, such inflation can arise due to a variety of factors such as  
97 uncorrected population structure, and is often addressed by rescaling  $\chi^2$  statistics by the

98 median inflation across the genome<sup>21,22</sup>. However, such rescaling is only appropriate if the  
99 great majority of the genome is unaffected by the biological signal being studied. If, instead,  
100 a substantial fraction of the genome has real signal<sup>21,23</sup>, random locations in the genome will  
101 not provide an appropriate neutral baseline. In fact, we find evidence of exactly this problem:  
102 a large proportion of the genome in linkage disequilibrium (LD) with sites with evidence of  
103 directional selection (Supplementary Information section 2, Extended Data Figure 2b).  
104

105 Instead, we calibrated our test by taking advantage of a striking finding about the connection  
106 between selection coefficients and associations to phenotypes in living people. We find that  
107 the proportion of SNPs showing significant association to a phenotype in a GWAS increases  
108 dramatically with our selection statistic Z, plateauing at around 3.9-times the rate of overlap  
109 for random SNPs (Figure 1a) (for this analysis we used 1,363,674 SNPs with a genome-wide  
110 significant association to at least one phenotype for 452 traits in the Pan-UK Biobank<sup>24</sup>). The  
111 increase is observed even after conditioning on minor allele frequency (MAF) to remove  
112 artifacts due to both selection and phenotypic associations being easier to detect for higher  
113 MAFs. The plateau occurs at the same place when we control for negative selection at linked  
114 loci (Extended Data Figure 3a). This is the pattern expected for a true threshold for genome-  
115 wide significance: if SNPs beyond this threshold reflect a combination of true signal and false  
116 discoveries, we would expect enrichment to continue beyond it. Because this threshold occurs  
117 at a value of Z=9.10—1.67-times larger than the standard threshold (5.45) for genome-wide  
118 significance for a normal distribution—we rescale the naïve score by this quantity to obtain  
119 an X-statistic (Z/1.67) whose significance threshold matches the standard threshold.  
120

121 To test whether we set an appropriate threshold for genome-wide significance with this  
122 procedure, we used orthogonal information: the sum of squared derived allele frequency in  
123 200 kilobase haplotypes linked to each tested allele: the “Haplotype Allele Frequency”  
124 (HAF) score. Previous work<sup>25,26</sup> showed that directional positive selection on derived alleles  
125 can increase HAF scores, while negative selection always decreases it, and we verified this  
126 by simulation (Extended Data Figure 3b, Supplementary Information section 3). After  
127 computing the residual HAF-score for each variant controlling for negative selection at linked  
128 loci<sup>27,28</sup>, we find it increases with the X-statistic and plateaus around 5.45, the standard  
129 threshold for genome-wide significance in GWAS (Figure 2b, Extended Data Figure 3c).  
130

131 To translate X to a posterior probability of selection  $\pi$ , we used a False Discovery Rate  
132 (FDR) approach (Supplementary Information section 2). We fit a smooth function to the  
133 enrichment curve for GWAS signals and estimate that at X-statistic magnitudes greater than  
134 our threshold for genome-wide significance of 5.45,  $\pi > 99\%$  (Extended Data Table 1).  
135

136 We confirmed that our X-statistics are detecting biologically meaningful patterns by showing  
137 that signals of selection are unusually associated with specific classes of traits<sup>29</sup>. In particular,  
138 we find enrichment for SNPs contributing to blood-immune-inflammatory traits (95%  
139 confidence interval (CI) 2.6-6.8)<sup>12,13</sup>, compared to random SNPs with matched characteristics  
140 defining the baseline of 1-fold. In contrast, for mental-psychiatric-nervous and behavioral  
141 traits, we do not see enrichment (95% CI of 0.2-1.3 and 0.5-1.4) (Figure 1c, Extended Data  
142 Figure 4a). These patterns cannot be explained by differences in allele frequencies or  
143 purifying selection since we control for these factors. The intensity of selection on blood-  
144 immune-inflammatory and cardio-metabolic traits increased in the Bronze Age relative to the  
145 pre-farming period (Figure 1c, Extended Data Figure 4b), which may reflect adaptation to  
146 new diets, higher population densities, or living closer to domesticated animals.  
147

148 **Hundreds of loci affected by directional natural selection**

149 We identified 347 independent loci (279 excluding the HLA region) with  $|X|>5.45$ ,  
150 corresponding to a  $\pi>99\%$  probability of selection (Figure 2a). To produce this list, we  
151 identified the strongest signal in the genome and considered all SNPs in LD with it in modern  
152 Europeans from the 1000 Genomes Project ( $r^2>0.05$ ) to potentially reflect the same signal.  
153 We then found the second-strongest signal excluding these positions, and so on until no more  
154 SNPs pass this threshold (Extended Data Figure 2b). We provide visualizations of the  
155 trajectories for these 347 loci (Supplementary Information section 5) and summary statistics  
156 for 9.9 million imputed variants (Online Table 4), which can be cross-referenced with GWAS  
157 and viewed along with their frequency trajectories at the AGES internet browser <https://reich-ages.rc.hms.harvard.edu>.  
158

159

160 The actual number of loci under selection is likely to be much larger. Using a threshold of  
161  $|X|=3.16$ , which corresponds to FDR=50%, we identify 10361 non-HLA loci, implying  
162 >5000 independent episodes of selection. Moreover, our approach to identifying distinct loci  
163 is conservative, because genuinely selected alleles in LD with nearby stronger ones will be  
164 missed. Down-sampling analyses show that further increases in sample size are expected to  
165 increase the number of loci further, with people living >8000 years ago providing the most  
166 added power (Extended Data Figure 1d,e).

167

168 To obtain insight into the phenotypic targets of the loci under natural selection, we take  
169 advantage of the fact that a high proportion (82%) of the variants with genome-wide evidence  
170 of selection are independently associated to a phenotype in at least one Pan-UK Biobank  
171 GWAS in living people. However, biological interpretation is complicated since the allele  
172 that was the target of selection may differ from the tag SNP we are using to represent the  
173 locus (and may even be in a neighboring gene), because some alleles affect multiple  
174 phenotypes, or because the relevant modern trait may not be measured in one of the GWAS  
175 we are analyzing, or because the phenotype in modern societies may not have existed in the  
176 ancient ones where selection acted. The median selection magnitude  $|s|$  at the tag SNPs is  
177 0.8% (range 0.4-4.2%), and the median minor allele frequency (MAF) is 19%. Standard  
178 errors in our estimates of  $|s|$  for common alleles are ~0.1%, and we have limited power to  
179 detect selection coefficients of magnitude <.5% (Figure 2b) (Extended Data Figure 1c).  
180

181

182 We compared our results to those of five previous selection scans in Holocene West Eurasia  
183 (four based on ancient DNA) (Table 1). Of 39 unique non-HLA loci that met the formal  
184 threshold for genome-wide significance in at least one of the previous studies, 17 pass our  
185  $\pi>0.99$  threshold. The other 22 do not replicate, in most cases due to what appears to be  
186 incompletely controlled population structure driven by mixtures of populations with different  
187 allele frequencies before they came together (Supplementary Information section 5). (Two of  
188 the previous studies also reported additional candidate loci that did not pass the author's own  
189 genome-wide significance threshold, and we found that only ~10% of these replicated,  
190 suggesting most are false-positives<sup>8,13</sup>.)

191

192 We present a gallery of 36 single-allele trajectories of particular interest (Figure 3) as well as  
193 estimates of how their selection coefficients changed over time (Extended Data Figure 5).  
194 These loci are not necessarily those with the largest X-scores, but are highlighted as they  
195 address long-standing debates. They include 24 passing the  $\pi>99\%$  threshold, 7 with  
196 probable evidence of selection ( $64\%<\pi<98\%$ ), and 5 with surprising negative findings.

197 HLB-DQB1: Selection in favor of the major risk factor for celiac disease (panel 1). At the  
198 HLA region of chromosome 6, densely packed genes play key roles in microbe recognition.  
199 rs3891176 (C>A, meaning that the ancestral allele is C and the newly arising mutation is A) is an excellent tag for *HLA-DQB1\*02/DQ2*, with individuals carrying two A alleles having a  
200 19-fold higher susceptibility for celiac disease or gluten sensitivity (Extended Data Figure  
201 6a,b). The A allele has a selection coefficient of  $s=4.5\%$  ( $\pi>99\%$ ), rising from ~0% to ~20%  
202 in the last 4000 years. These findings speak to the debate about the relationship between  
203 agriculture and celiac disease<sup>30-32</sup>, as the results suggest that the pathogenic exposures that  
204 drove its rise were not a phenomenon only or largely of the Neolithic.  
205

206  
207 ABO: Positive selection for B at the expense of the A allele (panel 2). *ABO* modifies  
208 oligosaccharides in glycoproteins on the surface of red blood cells and codes for the A, B,  
209 and null (O) alleles that interact in different ways with pathogens<sup>33,34</sup>. We show that the B  
210 allele rose from ~0% to ~10% over the last ~6000 years ( $s=2.9\%$ ,  $\pi>99\%$ ), and was matched  
211 by a concomitant decrease in A frequency. The A and B alleles are associated with opposite  
212 effects on many phenotypes, suggesting that with changing lifestyles and pathogenic  
213 exposures, the optimal balance of these alleles changed (Extended Data Figure 6c,d).  
214

215 TCHH: Selection for an allele that reduced male pattern baldness (panel 3). An allele at  
216 missense SNP rs11803731 (A>T) in *TCHH* is a strong predictor of straight hair and male  
217 pattern baldness in Europeans. The derived allele T is rare in African and East Asian  
218 populations, and has been hypothesized to have been positively selected, analogous to the  
219 straight-hair *EDAR* allele in East Asians<sup>35</sup>. We observe an opposite trend: the derived allele  
220 was negatively selected ( $s = -0.9\%$ ,  $\pi>99\%$ ), decreasing from ~50% to ~20% in the past 7000  
221 years. This implies a 1.8% decrease in predisposition to baldness over this period.  
222

223 TYK2. Reversal of selection at a major factor for tuberculosis (panel 4). Individuals carrying  
224 two copies of the rs34536443 G>C allele have >80% prevalence of clinically significant  
225 tuberculosis<sup>36</sup>. Previous work<sup>37</sup> found evidence of negative selection on the C allele and  
226 hypothesized it was associated with the time tuberculosis began to be endemic in Europe. We  
227 confirm a drop in frequency from ~9% to ~3% in the last ~3000 years ( $s = -2.3\%$ ,  $\pi>99\%$ ),  
228 but also identify positive selection from ~5500 to ~3000 years ago, from around ~2% to ~9%  
229 ( $s=2.6\%$ ,  $\pi>99\%$ ). This may reflect changing endemicity of different pathogens over time.  
230

231 HLA-DRB1. Elevated MS risk in north Europe is not due to selection on the steppe (panel 5).  
232 A previous study<sup>38</sup> discovered positive selection at the rs3135388 G>A tag SNP for the HLA-  
233 DRB1\*15:01 risk factor for multiple sclerosis (MS)<sup>39</sup>. Because selection was already  
234 occurring in Yamnaya steppe pastoralists, and Yamnaya ancestry is most common in north  
235 Europeans today, the authors argued that the genetically higher risk for MS in north than in  
236 south Europeans was driven by selection on the steppe. We confirm positive selection at this  
237 allele, rising from ~0% to ~18% between ~6000 and ~2000 years ago ( $s=4.0\%$ ,  $\pi>99\%$ ).  
238 However, we also document three features of the selection history missed by previous work  
239 (Supplementary Information section 6), and which together show that the primary driver of  
240 the north/south differential in this allele's frequency was not selection on the steppe. First,  
241 selection did not begin on the steppe<sup>38</sup>; it was occurring earlier south of the Caucasus  
242 mountains in people without steppe ancestry. Second, after Yamnaya ancestry spread west,  
243 selection was stronger in north Europe at  $s = 14.5 \pm 3.4\%$  than in southwest Europe at  $s = 5.1 \pm 2.5\%$  (measured >3500 BP). Third we document negative selection in the last ~2000 years  
244 missed by previous work ( $s = -2.4\%$ ,  $\pi>99\%$ ), likely reflecting new pathogen exposures.  
245

246

247 HFE: Reversal of selection at the major risk factor for hemochromatosis (panel 6). The  
248 rs1800562 (G>A) allele predicts pathogenic iron buildup in cells in individuals with two  
249 copies, and we find evidence of positive selection from ~5000 to ~2000 years ago, rising  
250 from ~1% to ~5% ( $s = 2.9\%$ ,  $\pi = 98\%$ ), then dropping to ~3% today. This reversal is not  
251 genome-wide significant ( $s = -1.6\%$ ,  $\pi = 29\%$ ), but is compelling as a single hypothesis test at  
252 a locus with long-standing speculation regarding selection. It was hypothesized that the  
253 causal allele protected against *Yersinia pestis* (the agent of Black Death)<sup>40</sup>, but this is unlikely  
254 as its frequency was decreasing by the time of the Justinianic and Medieval pandemics<sup>41,42</sup>.  
255

256 CCR5-Δ32: Positive selection at an allele conferring immunity to HIV-1 infection (panel 7).  
257 The *CCR5-Δ32* allele confers complete resistance to HIV-1 infection in people who carry two  
258 copies<sup>43–45</sup>. An initial study dated the rise of this allele to medieval times and hypothesized it  
259 may have been selected for resistance to Black Death<sup>46</sup>, but improved genetic maps revised  
260 its date to >5000 years ago and the signal became non-significant<sup>47,48</sup>. We find that the allele  
261 was probably positively selected ~6000 to ~2000 years ago, increasing from ~2% to ~8% ( $s$   
262 = 1.1%,  $\pi = 93\%$ ). This is too early to be explained by the medieval pandemic, but ancient  
263 pathogen studies show *Yersinia* was endemic in West Eurasia for the last ~5000 years<sup>49–51</sup>,  
264 resurrecting the possibility that it was the cause, although other pathogens are possible.  
265

266 Selection for light skin at 10 loci (panels 8–17). We find nine loci with genome-wide signals  
267 of selection for light skin, one probable signal, and no loci showing selection for dark skin.  
268

269 CFTR: No evidence of selection for the major cystic fibrosis risk allele ΔF508 (panel 18).  
270 The major risk allele for this recessive disease in Europeans<sup>52,53</sup> has been hypothesized to be  
271 an example of heterozygote advantage due to advantages in carriers such as resistance to  
272 cholera<sup>54</sup>. However, we find no evidence of selection ( $\pi < 1\%$ ), with the earliest direct  
273 observation at ~2200 years ago in Great Britain and the earliest imputed one ~10100 years  
274 ago in Anatolia. It seems unlikely that cholera was endemic in West Eurasia this long;  
275 another explanation is needed for the persistence of this allele which in two copies also  
276 causes male infertility.  
277

278 Fourteen other selection discoveries are highlighted in panels 19–32 of Figure 3. Most pass  
279 our threshold for genome-wide significance at  $\pi > 99\%$ : *TSBP1* (Celiac disease,  $s = 4.6\%$ );  
280 *HLA-DQB1* (Celiac disease,  $s = 1.1\%$ ); *HLA-DRB1* (Rheumatoid arthritis,  $s = -0.9\%$ ); *GYP4*  
281 (increases MNS blood group N,  $s = -0.9\%$ ); *DUOX2* (increases Ferritin level,  $s = 1.3\%$ );  
282 *SLC22A4* (Crohn's disease,  $s = 1.9\%$ ); *TLR1* (Leprosy resistance,  $s = 1.9\%$ ); *CYP1A2* (decreases  
283 blood pressure,  $s = 1.1\%$ ); *NADSYN1/DHCR7* (increases vitamin D,  $s = 0.9\%$ ); and *ADH1B*  
284 (lower risk for alcoholism,  $s = 2.6\%$ ). Four more signals are probable: *ABCG2* (gout,  $s = 0.9\%$ ,  
285  $\pi = 98\%$ ); *APOE* (hyperlipidemia,  $s = 0.9\%$ ,  $\pi = 80\%$ ); *GCKR* (hyperlipidemia/gout,  $s = 0.4\%$ ,  
286  $\pi = 65\%$ ), and *SERPINA1* (alpha-1 antitrypsin deficiency,  $s = 1.6\%$ ,  $\pi = 73\%$ ).  
287

288 Panels 33–36 highlight four negative signals at loci previously hypothesized to have been  
289 selected: a second locus at *SERPINA1* (alpha-1 antitrypsin deficiency); *PTPN22*  
290 (hypothyroidism); a second locus at *HFE* (hemochromatosis); and *IL23R* (Crohn's disease).  
291

## 292 **Directional selection shaped dozens of complex traits**

293 Having examined selection on individual loci, we searched for evidence that groups of alleles  
294 with similar influence on traits today trended in the same direction in the past, as would be  
295 expected if a phenotype with a similar genetic underpinning was the target of selection. To  
296 study this, we leveraged GWAS data for 452 mostly quantitative traits in the Pan-UK

297 Biobank, and 107 dichotomous traits from studies especially of common disease<sup>55</sup> (Online  
298 Table 5). How phenotypes manifest in modern societies may be very different from how they  
299 manifested in past populations living in different environments with different lifestyles, so  
300 any signals discovered by this approach should not be interpreted as evidence for selection on  
301 the exact phenotype being tested.  
302

303 We used three statistics to test for coordinated selection on alleles affecting the same trait.  
304 First, we computed a polygenic score (PGS) for each GWAS: a linear combination of allelic  
305 values, weighted by estimated effect size. We evaluated whether the change in PGS over time  
306  $\gamma$  (which we scaled so one-unit corresponds to a one standard deviation change over ten  
307 millennia) is more than could be expected by genetic drift alone. To test if the observed  
308 deviation is significant, we repeated the test 100 times with randomly flipped signs of GWAS  
309 effect sizes, to correct for LD among neighboring sites. As a second test, we repeated the  
310 procedure without using the magnitudes of the GWAS effects, and instead only the sign,  
311 generating a statistic  $\gamma_{\text{sign}}$  that may be less affected by concerns about transferability of PGS  
312 across groups<sup>12,56–58</sup>. Third, we performed a SNP-by-SNP comparison for each trait, using  
313 cross-trait LD Score Regression (LDSC) to estimate genetic correlation ( $r_s$ ) between selection  
314 summary statistics and GWAS summary statistics<sup>59</sup>, accounting for non-independence of  
315 SNPs. We computed a standard error from a Block Jackknife to test if this correlation is  
316 significantly different from zero. We find high Pearson's correlation for all three tests (75–  
317 91%; Extended Data Figure 7).  
318

319 For 31 of the 559 traits examined, we were able to carry out a further test of robustness by  
320 leveraging data from East Asian GWAS. Early studies claimed selection for greater height in  
321 north than in south Europeans, but this was later shown to be a false-positive due to  
322 uncorrected population structure in GWAS (ancestry differentially carried by north and south  
323 Europeans) that is correlated to structure in the groups tested for selection<sup>60,61</sup>. However,  
324 population structure in East Asia should be almost completely uncorrelated to that in the  
325 ancient West Eurasians, so it is difficult to see how validation by this test could be anything  
326 but a real signal of selection<sup>12,56</sup>.  
327

328 We identified 12 traits with significant signals from all three tests after correction for number  
329 of traits tested ( $p < 10^{-4}$ , correcting for ~500 hypotheses) (Figure 4, Extended Data Figure 8).  
330

331 One of the strongest signals is an increase over time in the PGS for light skin pigmentation ( $\gamma$   
332 =  $1.77 \pm 0.13$  standard deviations increase in mean PGS in ten millennia,  $P = 3.0 \times 10^{-45}$ ; Figure  
333 4, Extended Data Figure 8). This plausibly reflects selection for increased synthesis of  
334 vitamin D in regions of low sunlight in farmers with little of it in their diets. Previous ancient  
335 DNA analysis<sup>57</sup> found most of the phenotypic shift is driven by a few loci. Our results agree:  
336 50% of the shift is due to *SLC45A2* alone, and 69% by the top 7 loci (Extended Data Figure  
337 9). However, the selection was extraordinarily polygenic as we need to drop the top 104 loci  
338 before the signal disappears (Extended Data Figure 10). A model in which selection for  
339 pigmentation impacted all variants in proportion to their effect size fits the data ( $P = 0.10$ ).  
340

341 Type 2 diabetes risk factors give compelling signals of negative selection. Thus, we observe  
342 negative selection on combinations of alleles that today increase body fat percentage ( $\gamma = -$   
343  $1.03 \pm 0.15$ ), waist circumference ( $\gamma = -1.04 \pm 0.15$ ), and waist-to-hip ratio ( $\gamma = -0.80 \pm$   
344  $0.14$ ), supporting the “Thrifty Gene” hypothesis that a genetic adaptation to store fat in times  
345 of plenty, became deleterious after the transition to food-production (Figure 4). For type 2

346 diabetes itself, the signal ( $\gamma = -0.40 \pm 0.11$ ) just misses the multiple hypothesis-testing  
347 corrected threshold, but the other two exceed it ( $\gamma_{\text{sign}} = -0.51 \pm 0.12$ ;  $r_s = -0.16 \pm 0.04$ ).  
348

349 We find signals of negative polygenic selection against alleles associated today with  
350 psychoses such as bipolar disorder ( $\gamma = -0.67 \pm 0.14$ ) and schizophrenia ( $\gamma = -0.84 \pm 0.14$ )  
351 (Figure 4). Superficially this is in tension with the finding that variants with genome-wide  
352 significant of selection are not enriched for variants known to modulate psychiatric traits  
353 (Figure 2b). However, for variants with weaker signals, we do observe heritability  
354 enrichment (Extended Data Figure 4a). Brain traits have qualitatively different genetic  
355 architectures than blood-immune-inflammatory ones, with a higher total proportion of sites  
356 modulating them and smaller effect sizes on average per allele<sup>62</sup>. If brain traits tend to be  
357 associated with many alleles with small selection coefficients, this may reduce heritability  
358 enrichment at precisely the loci in the genome giving the strongest selection signals. These  
359 traits too are extraordinarily polygenic: we have to drop 740 loci for bipolar disorder and 726  
360 loci for schizophrenia for the signals to become non-significant (Extended Data Figure 10).  
361

362 We observe signals of selection for combinations of alleles that at today associated with  
363 healthy lifestyles into old age. This includes selection for alleles that promote faster walking  
364 pace ( $\gamma = 0.99 \pm 0.14$ ), against alleles that today are associated with smoking ( $\gamma = -0.54 \pm$   
365  $0.14$ ), and against alleles contributing to overall health decline ( $\gamma = -1.00 \pm 0.14$ ).  
366

367 We finally observe signals of selection for combinations of alleles that today predict three  
368 correlated behavioral traits: scores on intelligence tests (increasing  $0.79 \pm 0.14$ ), household  
369 income (increasing  $1.11 \pm 0.14$ ), and years of schooling (increasing  $0.61 \pm 0.13$ ). These  
370 signals are all highly polygenic, and we have to drop 463 to 1109 loci for the signals to  
371 become nonsignificant (Extended Data Figure 10). We also tested for a correlation of East  
372 Asian GWAS effect size measurements to West Eurasian selection. We observe a significant  
373 correlation for  $\gamma_{\text{sign}}$  ( $P=3.8 \times 10^{-6}$ ) and  $r_s$  ( $P=1.9 \times 10^{-10}$ ) (Extended Data Figure 11), which is  
374 very difficult to explain as an artifact of population structure.  
375

376 There are caveats when interpreting signals of polygenic adaptation, especially for the three  
377 genetically correlated traits of scores on intelligence tests, household income, and years of  
378 schooling. These traits—for which there is evidence of significant negative selection in the  
379 last century, for example in Iceland, in the opposite direction to the long-term increase we  
380 detect<sup>63–65</sup>—are only relevant to modern societies, and would have been unmeasurable in the  
381 preliterate societies over the vast majority of the period during which selection acted. The  
382 difficulty of interpretation is enhanced by the fact that the alleles driving down the frequency  
383 of type 2 diabetes-related traits, are highly correlated to those contributing to the increased  
384 scores for years of school, household income, and intelligence tests (Extended Data Figure  
385 12). We could not gain meaningful additional insight into the selection mechanism by  
386 repeating analyses in family-based GWAS<sup>66</sup> due to the limited sample sizes in these studies  
387 (Extended Data Figure 13).  
388

389 **Discussion**

390 Previous work has shown that classic selective sweeps driving alleles to fixation have been  
391 rare over the broad span of human evolution<sup>67,68</sup>. Thus, we were surprised that over the last  
392 14,000 years in West Eurasia there have been many hundreds of instances of directional  
393 selection with coefficients on the order of 0.5% or more (Figure 2b). This is large enough that  
394 if a similarly dense landscape of directionally selected variants had existed tens of thousands  
395 of years ago, and if the selection coefficients had been constant since then, we would expect

396 many fixed differences across populations, despite the fact that previous studies have shown  
397 there are only a handful—hardly more than would be expected based on random drift<sup>68</sup>.  
398

399 The simplest way to resolve this paradox is to recognize that selection coefficients are  
400 unlikely to have been constant over time, even though we make this simplifying assumption  
401 to make it possible to detect selection. By sliding a 2000-year window through our time  
402 transect and re-estimating selection coefficient within each window, we can already see that  
403 there have in fact been changes in selection pressures at a number of the loci we analyze  
404 (Extended Data Figure 6), including at *HLA-DRB1*, *TYK2* and *HFE* (Figure 3). By comparing  
405 the estimated age of the mutation that contributed each selected allele<sup>9</sup>, to the extrapolated  
406 time to reach fixation given its estimated *s*-value, we find that around half of the mutations  
407 have true ages an order of magnitude larger than the expected sweep age, which means that  
408 selection coefficients on the alleles must have shifted over time (Figure 2c).  
409

410 An alternative explanation for this paradox is to hypothesize that West Eurasians have been  
411 experiencing qualitatively more and different natural selection in the Holocene than in earlier  
412 periods because of rapidly changing lifestyles and economies. Without a comparable time  
413 transect before the advent of food production and societies with high population densities, it  
414 is impossible to test this directly. However, this hypothesis is consistent with our evidence of  
415 particular intense selection for blood-immune-inflammatory traits, and our evidence that  
416 selection for these traits becoming even stronger in the Bronze Age than it was in earlier  
417 periods (Figure 1c, Extended Data Figure 4b).  
418

419 We project that there are at least 5000 independent signals of directional selection (half of the  
420 10361 non-HLA loci found at the FDR=50% threshold) that are in linkage disequilibrium  
421 with the overwhelming majority of variants in the genome (Extended Data Figure 2b). This  
422 seem to be at odds with findings that there has been relatively little contribution from  
423 directional selection to allele frequency changes in genome compared to much larger forces  
424 of gene flow, genetic drift, and purifying or stabilizing selection<sup>69</sup>. In fact, there is no conflict.  
425 Our method allows us to partition the effects of selection at each SNP into the effects of  
426 directional selection (*s*), and the combined effects of fluctuating selection and drift ( $\sigma^2$ ). We  
427 estimate that only  $2.35 \pm 0.13\%$  (jackknife standard deviation) of allele frequency changes  
428 are due to directional selection. These results suggest that selection is so rampant that even if  
429 a tiny fraction of allele-frequency change is due to directional selection, this corresponds to  
430 many hundreds of loci. A corollary is that recent studies finding that stabilizing selection is  
431 relatively more important than directional selection in shaping the human allele frequency  
432 spectrum<sup>70</sup> are fully reconcilable with our analyses.  
433

434 It is important to apply similar approaches to ancient DNA time series over longer times and  
435 to other world regions. Comparison of ancient DNA time transects would allow more  
436 generalizable insights by identifying which patterns of selection are shared and which are  
437 distinctive to the human population history of Holocene West Eurasia.

## Methods

438 **Testing for selection while correcting for population structure**  
439 We used a generalized linear mixed model (GLMM) approach to correct for population  
440 structure, a major confounder in scans for significant changes in frequency over time  
441 especially as major migration and population mixture have been common in almost all parts  
442 of the world. Previous studies have corrected for structure in ancient DNA time transects by  
443 modeling the population history and estimating mixture proportions, which works optimally  
444 only if there are data from the true source population, which is rarely the case. It is tempting  
445 to use an unsupervised approach like Principal Component (PC) to address population  
446 structure. However, after experimentation we found this is not effective as PCs are correlated  
447 with sample dates which creates collinearity with the quantity we are most interested in (the  
448 time-varying component), inflating the empirically estimated variance and reducing power.  
449

450 The mixed model approach, which is often deployed in the context of genetic association  
451 studies to address similar challenges<sup>71</sup>, offers a way to address these issues by combining the  
452 structured data in an unsupervised manner and estimating fewer parameters over a wider span  
453 of time which results in greater power compared to employing separate regression analyses  
454 for each population or comparing the estimated means from different groups. Our simulations  
455 show that under simplifying assumptions, a GLMM is more powerful in controlling for  
456 population structure and detecting change in allele frequency compared to a generalized  
457 linear model using the top principal components (PC) as covariates (Extended Data Figure  
458 14). Thus, despite the fact that the model fitted by the GLMM is far from that expected under  
459 true selection, and will miss real signals at sites with fluctuating selection like *TYK2*  
460 rs34536443, the method has advantages, and we found in practice that it detected many loci.  
461

462 We used our GLMM to fit a linear time-varying component to the logit (log-odds)  
463 transformation of allele frequency at each position in the genome, and then to test if there is  
464 evidence for a consistent trend in allele frequency change over time for all populations. We  
465 search for evidence of such a trend beyond the prediction based on population structure and  
466 associated genetic drift relating sampled individuals in space and time as measured by the  
467 covariance of genotypes over all the individuals, known as the Genetic Relationship Matrix  
468 (GRM). In our GLMM, the response variable for each tested allele  $j$  is the allele count. The  
469 allele counts for an individual  $i$  are drawn from a binomial distribution  $B(2, p_{ij})$ , where 2 is  
470 the number of chromosomes each person carries at each position, and  $p_{ij}$  is the unknown  
471 frequency of allele  $j$  in the population in which the tested individual  $i$  lives. A logit link  
472 function allows the frequency  $p_{ij}$  to be modeled as a linear combination of covariates. This is  
473 a generalization of the Logistic Mixed Model where the response variable is binary:

$$\ln\left(\frac{p_{ij}}{1-p_{ij}}\right) = \alpha_j + s_j t_i + MVN(0, \sigma_j^2 \mathbf{K}), \quad (1)$$

474 The logit function,  $\ln\left(\frac{p_{ij}}{1-p_{ij}}\right)$ , transforms allele frequency so its expected change per  
475 generation is proportional to the selection coefficient  $s_j$  (regardless of  $p_{ij}$ )<sup>72,73</sup>.  $\alpha_j$  is a constant  
476 related to the average logit transformation of allele frequency in sampled individuals at time  
477  $t=0$  today.  $s_j$  is the per-generation selection strength at the allele, assumed constant over time  
478 and space during the period of our time transect; our test for selection is simply a test for  
479 whether the equation fits significantly better if  $s_j$  is non-zero than if it is zero.  $t_i$  is the  
480 negative sampling date in the past, in units of twice the generation interval<sup>72,73</sup> (assuming 29  
481 years per generation).  $g_{ij}$  is a random effect, an error term capturing individual-specific

482 variability not explained by fixed effects ( $\alpha_j + s_j t_i$ ). It differs from the error term in a  
483 Generalized Linear Model, which is independently and identically distributed following a  
484 normal distribution. In our GLMM, the error term is drawn from the vector  
485  $\mathbf{g}_j \sim MVN(0, \sigma_j^2 \mathbf{K})$ , following a multivariate normal distribution, where  $\mathbf{K}$  is the covariance  
486 matrix structure (the GRM), the empirically observed relatedness of all individuals to each  
487 other, and  $\sigma_j^2$  measures the drift at that variant.  
488

489  $s_j$ ,  $\sigma_j^2$  and  $\alpha_j$  are independently estimated for each of 9.9 million variants. Refitting them  
490 without being constrained by the values at other variants means the methodology is robust to  
491 false-positives due to processes that vary across SNPs such as degree of background selection  
492 which increases the effective amount of random genetic drift or variation in minor allele  
493 frequency (MAF); these nuisance random effects are soaked up by allowing  $\sigma_j^2$  and  $\alpha_j$  to  
494 vary, allowing us to test for a time-dependent influence on allele frequency fluctuations  $s_j$   
495 beyond what can be explained by the GRM. Our test for a non-zero  $s_j$  is thus a test for  
496 selection above and beyond what could be explained not just by structure but also other non-  
497 time-dependent processes. The penalty we pay for estimating variance components at  
498 millions of SNPs—in contrast to the constant variance component assumption used in mixed  
499 model analysis in Genome-Wide Association Studies (GWAS)<sup>71</sup>—is computational load. We  
500 grouped individuals with similar ancestry and dates into 3000 clusters (Supplementary  
501 Information section 7); at this resolution, our method required ~140,000 CPU hours.  
502

503 Using the GLMM, we obtain a point estimate for the selection coefficient at each variant and  
504 its standard error, and a Z-score for the number of standard errors this is from zero, a naïve  
505 test for selection. In practice, the statistic needs recalibration as it is inflated due to  
506 unmodeled features of the data, so we empirically assess significance from enrichment of  
507 signals in independent GWAS (Supplementary Information section 2).  
508

#### 509 **Fitting the generalized linear mixed model (GLMM)**

510 We developed PQLseq2, a faster implementation of PQLseq<sup>74</sup> for fitting the GLMM to count  
511 data. Despite a 27-fold speed increase, running a GLMM on ~15,000 individuals for ~9.9  
512 million variants was infeasible given our resources. To make analysis tractable, we grouped  
513 individuals into clusters of individuals with similar ancestry and coming from similar times.  
514

515 To identify the  $T = 3000$  clusters we analyze, we required there to be a maximum date gap  $G$   
516 = 500 years between any two individuals in each cluster. We initialized the interval  $I = (l=2,$   
517  $r=T)$  with midpoint  $m$ . We applied hierarchical clustering on the top 30 principal components  
518 (PCs) using the `sklearn.cluster.AgglomerativeClustering` function in Python with default  
519 parameters and  $n\_clusters = m$ . For each of the  $S$  clusters from the previous step, we  
520 performed hierarchical clustering on the dates with  $distance\_threshold = G$  and  $n\_clusters =$   
521 None. If the resulting number of clusters was larger than  $T + 1$ , we repeated the process with  
522  $I = (l, m)$ . If it was less than  $T - 1$ , we updated  $I = (m, r)$ . We repeated these steps until the final  
523 number of clusters was within  $T - 1$  to  $T + 1$ . Across 3,000 clusters, the individuals per cluster  
524 has a first quartile of 1, a median of 3, a third quartile of 6, and a maximum of 46.  
525

526 We use the same GLMM model as for the single variant analysis. However, the cluster can  
527 include more than one individual. The allele counts for each cluster  $i$  are drawn from a  
528 binomial distribution  $B(2n_i, p_{ij})$ , where  $n_i$  is the number of diploid individuals in the cluster,  
529 and  $p_{ij}$  unknown frequency of allele  $j$  in the population where individuals in cluster  $i$  reside.  
530

531 **Proportion of variance explained by directional selection**

532 The proportion of variance in allele frequency on the logit scale for each SNP  $j$  is:

$$\text{Proportion of variance for SNP } j = \frac{s_j^2 \cdot \text{var}(t)}{s_j^2 \cdot \text{var}(t) + \sigma_j^2} \quad (2)$$

533 We used 1000 independent SNPs, randomly selected across the genome with pairwise LD ( $r^2$ )  
534 less than 0.05, to estimate that directional selection explains an average of 2.35% of the  
535 variance in allele frequency, with a standard error of 0.13% based on jackknife estimation.  
536 The GLMM used for this analysis is based on the full sample size, rather than clustering  
537 individuals according to their ancestry and date.  
538

539 **Covariance structure for the GLMM**

540 The covariance structure matrix  $\mathbf{K}$  for clusters  $m$  and  $n$  is defined as:

$$K_{mn} = \frac{1}{N_m N_n} \sum_{i \in c_m} \sum_{j \in c_n} A_{ij} \quad (3)$$

541 Where  $c_m$  is the set of individuals in cluster  $m$ ,  $N_m$  is the number of individuals in cluster  $m$ ,  
542 and  $A_{ij}$  is the genetic relationship matrix (GRM) between individuals  $i$  and  $j$  and defined as<sup>17</sup>:

$$A_{ij} = \frac{1}{M} \sum_{k=1}^M \frac{(G_{ik} - 2f_k)(G_{jk} - 2f_k)}{2f_k(1-f_k)} \quad (4)$$

543 Here  $G_{ik}$  is the genotype for SNP  $k$  of individual  $i$ ,  $f_k$  is the allele frequency of SNP  $k$ , and  
544  $M$  is the number of SNPs. We created a GRM using all autosomal SNPs and applied a leave-  
545 one-chromosome-out (LOCO) scheme to prevent proximal contamination<sup>75,76</sup>, creating a  
546 separate GRM for each chromosome.  
547

548 **Polygenic score computation**

549 The polygenic score (PGS) is a weighted average of genotypes for  $M$  independent variants.

$$PGS_i = \sum_{j=1}^M w_j G_{ij} \quad (5)$$

550 Here,  $G_{ij}$  is the genotype for SNP  $j$  of individual  $i$  and  $w_j$  is the SNP weight. We generate  
551 four variations of the PGS score by including or excluding the HLA region, and utilizing the  
552 GWAS effect values ( $\beta_i$ ) or only the sign of the effects,  $\text{sign}(\beta_i)$ , as weights. For each  
553 phenotype, we generate an independent set of SNPs using a two-step clumping and  
554 thresholding process. Initially, we clump SNPs with PLINK using a P-value  $< 10^{-3}$ ,  
555  $r^2 < 0.05$ , and a 500 kb window. Then, we select the SNP with the smallest P-value as the  
556 index SNP, remove SNPs with  $D' > 0.2$  within 500 kb, and repeat until no SNP remains.  
557 Consequently, all remaining SNPs have  $P < 0.001$ , and if two SNPs are within 500 kb, their  $r^2$   
558  $< 0.05$  and  $D' < 0.2$ . To minimize residual population structure, we use the linear mixed  
559 model (LMM),

$$y_i = \alpha + t_i \gamma + g_i + e_i \quad (6)$$

560 Here,  $y_i$  is the polygenic score of the sample  $i$ , centered at zero and scaled by the standard  
561 error of PGS of the modern samples;  $t_i$  is the date scaled down by -10000 (so it is in units of  
562 ten millennia);  $\alpha$  is the intercept;  $\mathbf{g} \sim MVN(0, \sigma_g^2 \mathbf{K})$  is a vector of random effects where the

563 covariance structure matrix  $\mathbf{K}$  is the genetic relationship matrix; and  $\mathbf{e} = MVN(0, \sigma_e^2 \mathbf{I})$  is a  
564 vector of residual errors where  $\mathbf{I}$  is the identity matrix. The coefficient  $\gamma$  is the change of the  
565 polygenic score over 10000 years in unit of standard deviation from the zero-centered PGS of  
566 the modern samples. We use the coefficient  $\gamma$  as a proxy for directional polygenic selection.  
567

### 568 **Fitting the linear mixed model (LMM)**

569 We used GEMMA (v0.98.5)<sup>77</sup> to fit the LMM and estimate the polygenic selection  
570 coefficient ( $\gamma$ ). The running time was tractable, so we did not apply the clustering algorithm  
571 used in the GLMM analysis. We used the genetic relationship matrix as the covariance  
572 structure matrix  $\mathbf{K}$ . Here, PGS is calculated over all autosomes, and we could not use the  
573 LOCO approach from single-variant GLMM to avoid influence from neighboring positions.  
574 Instead, we used 80,085 high-quality, independent SNPs generated by the 'indep-pairwise  
575 1000 1 0.05' option of PLINK2 to calculate a GRM, using this as a covariance structure in the  
576 LMM to handle population structure and reduce proximal contamination.  
577

### 578 **Analyzing correlation between GWAS summary statistics and selection coefficients**

579 We use LD score regression (LDSC) version 1.0.1<sup>23,29,59</sup> to calculate the genetic correlation  
580 between GWAS summary statistics and the estimated selection coefficient. We use the pre-  
581 calculated LD scores computed using individuals of European ancestry from the 1000  
582 Genomes Project, which are provided with the LDSC software. To compute trans-ethnic  
583 genetic correlation, we used S-LDXR software<sup>78</sup>. We used the pre-calculated reference files  
584 for European and East Asian populations that are provided with this software.  
585

### 586 **Studying heritability enrichment and computing standardized effect size ( $\tau^*$ )**

587 We utilized stratified LD score regression (S-LDSC)<sup>29</sup> to estimate the contribution of each  
588 annotation to the heritability of polygenic traits. The set of annotations of interest was  
589 combined with the baseline-LD model (v2.2), which includes 97 annotations modeling minor  
590 allele frequency (MAF), linkage disequilibrium (LD), and functional architectures including  
591 coding regions, promoters, enhancers, and conserved elements<sup>29,79,80</sup>. Heritability enrichment  
592 quantifies the effects of the annotation. It is defined as the proportion of heritability explained  
593 by SNPs in the annotation divided by the proportion of SNPs in the annotation. The  
594 standardized effect size ( $\tau^*$ ) measures the effects unique to the focal annotation after  
595 conditioning on all the other annotations in the baseline-LD model<sup>67</sup>.  
596

### 597 **Adjusting for residual inflation in directional polygenic analysis**

598 To adjust for residual inflation in the estimated  $Z_\gamma$  for each trait, we carried out 100  
599 randomizations for each trait of interest, using the same SNPs employed for calculating the  
600 PGS of that trait and randomly assigning a weight of +1 or -1 to each SNPs for each  
601 simulation. The simulated PGS is not expected to show a signal of selection, as the weights  
602 are randomly flipped and should cancel for polygenic traits. Therefore, for each trait, we  
603 define an inflation factor by calculating the ratio of the median  $Z_\gamma^2$  for the simulation to the  
604 median of the chi-square distribution with 1 degree of freedom (0.455). If the inflation factor  
605 exceeds the median of 3.13 across all traits, we apply the median value as the correction  
606 factor for the test statistics. This allows us to carry out a valid analysis of polygenic signals  
607 driven by only a few SNPs under strong selection, which can cause a large inflation factor.  
608

### 609 **Simulation of genotypes**

610 To simulate the genotypes of individuals for a variant with a selection coefficient  $s_j$ , we used  
611 a random sample drawn from a Gaussian distribution with a covariance matrix of  $\sigma_j^2 K$ . We

612 estimated the genetic relationship matrix A using real data, and randomly selected  $\sigma_j^2$  from  
613 an empirical distribution. This distribution was derived by applying a GLMM to real data,  
614 specifically for 1000 randomly chosen SNPs, without clustering. We employed equation 1 to  
615 simulate different selection coefficients and determined the initial allele frequency by  
616 drawing from an empirical distribution of allele frequency in modern samples. We used this  
617 value as a constraint to define the constant  $\alpha_j$ . To sample genotypes, we drew from a  
618 binomial distribution, with the probability of the alternative allele calculated using the  
619 standard logistic function applied to both sides of equation 1.  
620

## 621 Sources of data for 8433 ancient individuals

622 We restricted to 8433 ancient individuals living between longitude 25W and 60E and latitude  
623 35N to 80N (Online Table 1). For 3644 ancient individuals, the sequences we analyze are  
624 published in other papers<sup>11,81–196</sup> and are reanalyzed here. For 244 ancient individuals, we  
625 newly publish shotgun sequencing data obtained on Illumina instruments on libraries for  
626 which either in-solution enrichment data from the same ancient DNA samples, extracts, or  
627 libraries was previously published; the present study serves as the formal report of these new  
628 sequences, and reanalysis of the data presented here should cite both the present study and the  
629 study that originally reported data from these individuals. Online Table 2 lists these samples  
630 along with newly reported shotgun data for an additional 56 anonymized newly reported  
631 individuals (for a total of 300 newly reported shotgun genomes which have a median of 4.87-  
632 fold coverage and of which 40 have at least 17-fold coverage).  
633

634 For 74 ancient individuals, we publish higher coverage in-solution enrichment data based on  
635 additional extracts, libraries and sometimes recaptures of libraries for which smaller amounts  
636 of in-solution enrichment data from the same samples were previously published, obtained by  
637 adding data from 155 newly reported ancient DNA libraries (Online Table 3). The present  
638 study serves as the formal report of these merges of previously published data with the newly  
639 generated data. Reanalysis of the data presented here should cite both the present study and  
640 the study that originally reported data from these individuals.  
641

642 For 4471 never-before-reported ancient individuals obtained by sequencing 5227 newly  
643 reported ancient DNA libraries (Online Table 3), we release raw ancient DNA data with  
644 permission of sample custodians. The individuals are anonymized, with the only information  
645 provided about them being point estimates of their dates and broad geographic categorization  
646 into five regions of West Eurasia. Analyses of population history and presentation of full  
647 archaeological information will be provided in subsequent studies and we request that the  
648 research community respects “Fort Lauderdale principles”<sup>15</sup>, allowing the generators of the  
649 data to report the first population history analyses. Any researchers are welcome to analyze  
650 the full dataset for studies of natural selection.  
651

## 652 Sources of data for contemporary individuals

653 We analyzed data from 6,510 contemporary individuals, comprising 5,935 from the UK  
654 Biobank<sup>19</sup>, 503 from the 1000 Genomes Project<sup>18</sup>, and 72 from published studies<sup>174,197–201</sup>.  
655

656 For the UK Biobank data, we selected individuals genotyped on the UK Biobank Axiom  
657 array, excluding those sequenced on the UK BiLEVE array to minimize batch effects. To  
658 ensure broad representation across Western Eurasia, we subsampled the UK Biobank,  
659 limiting the selection to at most 300 people per "country of birth" within Western Eurasia,  
660 focusing on countries with ancient DNA in this study. This yielded 6,088 individuals.  
661

662 For the remaining individuals, we calculated the Mahalanobis distance P-value based on the  
663 top 20 principal components, assuming the squared Mahalanobis distance follows a  $\chi^2$   
664 distribution with 20 degrees of freedom. Samples with P-values below the Bonferroni-  
665 corrected threshold of 8.2e-6 were removed, resulting in a final set of 5,935 individuals from  
666 58 countries, with a median of 55 and a mean of 102 individuals per country. These principal  
667 components were derived from the full set of UK Biobank samples.  
668

#### 669 **Ancient DNA data generation**

670 The great majority of wet laboratory work was performed in the ancient DNA laboratory at  
671 Harvard Medical School in Boston, USA, following established protocols that evolved over  
672 time from mostly manual processing (sample preparation, DNA extraction with silica  
673 columns<sup>202,203</sup> and partial UDG treated double-stranded library preparation<sup>204,205</sup>; capture was  
674 automated using a Perkin Elmer EP3 or Agilent Bravo NGS Workstations<sup>11,206,207</sup>) to mostly  
675 automated processing (DNA extraction<sup>208</sup>, double- and single-stranded library preparation<sup>209</sup>,  
676 capture, pooling for sequencing). New libraries (if not deeply shotgun sequenced) were  
677 enriched with the Twist Ancient DNA panel<sup>193</sup>, whereas older libraries were enriched with  
678 the 1240k reagent (or its predecessor, 390k and 840k). We sequenced on an Illumina  
679 NextSeq500 instrument until 2019, when we switched to an Illumina HiSeq X10 instrument,  
680 and finally to an Illumina NovaSeq X instrument in 2022. Archaeologists or collaborators  
681 from other ancient DNA laboratories in some cases provided sample powder, DNA extracts,  
682 or libraries, which we continued to process. Online Table 3 provides summary statistics based  
683 on in-solution enrichment for 5382 ancient DNA libraries for which we newly report data.  
684

#### 685 **Ancient DNA bioinformatic processing**

686 Most of the newly reported data come from sequencing the products of in-solution  
687 enrichment targeting a set of more than a million known polymorphisms<sup>193,207</sup>. In-solution  
688 enrichment extracts more information by enriching sequenced molecules to overlap sites that  
689 are polymorphic in humans (which also helps to greatly reduce the proportion of non-  
690 endogenous bacterial/microbial sources that colonized the samples post-mortem). The great  
691 majority of ancient DNA libraries we analyzed are marked with identification tags (barcodes  
692 and indices) before sequencing in pools. We merged paired-end sequences, requiring that  
693 there is no more than one mismatch in the overlap between paired sequences where the base  
694 quality is at least 20 or three mismatches if the base quality is <20. We did not analyze  
695 sequences we could not merge. We stripped adapters and identification tags to prepare  
696 molecules for alignment. A custom toolkit (<https://github.com/DReichLab/ADNA-Tools>)  
697 was used for all these steps. We aligned merged sequences to the hg19 version of the human  
698 reference genome with decoy sequences (hs37d5) using the single-ended aligner, BWA  
699 SAMSE v.0.7.15<sup>210</sup> with typical ancient DNA alignment parameters -n 0.01 -o 2 and -l 16500  
700 which disables pre-alignment seeding. Duplicate reads were marked using Picard  
701 MarkDuplicates (v.2.17.10)<sup>211</sup>. In addition, merged sequences are also mapped with the same  
702 parameters as the Reconstructed Sapiens Reference Sequence (RSRS)<sup>212</sup>, which enables  
703 mitochondrial-specific metrics. Our bioinformatic processing produces data and key metrics,  
704 including estimates of authenticity based on elevated damage rates at the end of sequences  
705 (indicative of ancient DNA), contamination rates, and endogenous rates. A subset of libraries  
706 that had a very high proportion of human DNA were additionally shotgun sequenced to  
707 generate coverage throughout the genome and underwent the same bioinformatics processing.  
708

#### 709 **Imputation**

710 To carry out imputation, we used as input either data from ancient individuals (mapped  
711 sequences) or modern individuals (SNP array genotypes), and then used allelic correlation  
712 patterns in a haplotype reference panel<sup>18,213</sup> to predict genotypes at millions of sites.  
713

714 In detail, for each sample we used bcftools mpileup (v1.13)<sup>214</sup> to generate genotype  
715 likelihoods for all variants (SNPs and indels) in the panel. We used the high coverage (30x)  
716 1000 Genomes Project<sup>18</sup> phase 3 sequences as the reference panel and converted the  
717 assembly version to GRCh37/hg19 using CrossMap (v0.5.2)<sup>215</sup>. We kept 2504 unrelated  
718 samples and biallelic variants that pass all the quality control filters reported by gnomAD  
719 (v2.1.1)<sup>216</sup>. We used GLIMPSE (v1.0.0)<sup>20</sup> with the reference panel to impute and phase each  
720 sample individually. Due to higher reference bias for indels, we ignored their genotype  
721 likelihood, set them to missing, and passed this to GLIMPSE to impute all biallelic autosomal  
722 SNPs and indels based on genotype likelihood of SNPs and haplotype information for both  
723 SNPs and indels in the reference panel. This means we only use reference panel information  
724 to impute indels even where we have sequences overlapping the indels. After imputation is  
725 done, we add the genotype caller information of all variants (SNPs and indels) to the final bcf  
726 file.  
727

728 To minimize discrepancies between imputation of ancient DNA and UK Biobank data, we re-  
729 imputed the UK Biobank genotyping data. We utilized Affymetrix confidence files to  
730 simulate genotype likelihoods and processed these through the same imputation pipeline  
731 employed for ancient DNA.  
732

### 733 Sample quality control

734 For each imputed sample, we define imputation quality score  $IQS = \text{mean}(GP_1 | GT = 1)$ ,  
735 where  $GT$  is the most likely genotype based on the imputed genotype posterior  $\mathbf{GP} =$   
736  $(GP_0, GP_1, GP_2)$  and  $\sum_{i=0}^2 GP_i = 1$ . We only kept samples with high imputation quality score  
737  $IQS > 0.9$ . We used KING to detect duplicates and related samples up to the second degree.  
738 We prioritize samples by their IQS and drop relatives up to the second degree until there are  
739 no two samples that are second-degree related or closer. We also fit a linear regression model  
740 to the top 100 PCs as explanatory variables and used the reported date of samples as the  
741 response variable to remove outliers where reported and predicted date are very different.  
742 Sample quality control is described in detail in Supplementary Information section 1.  
743

### 744 Variant quality control

745 The data analyzed in this study come from multiple sources and sequencing technologies:  
746 imputed ancient DNA sequences (shotgun sequences and enrichment for more than a million  
747 SNPs), European ancestry individuals largely from the 1000 Genomes Project, and imputed  
748 individuals of Western Eurasian ancestry from the UK Biobank genotyped using the UK  
749 Biobank Axiom Array. Variant quality control involved a two-step procedure. Initially, we  
750 applied brute-force filtering to compute principal components, allowing for the identification  
751 of ancestry-matching samples across datasets with similar allele frequencies. We filtered out  
752 variants if their allele frequencies differed strongly between sample sets, with the goal of  
753 minimizing batch effects from combining samples from different sources. This results in  
754 9,926,484 variants, including 8,212,921 SNPs and 1,713,563 indels, passing the final variant  
755 QC out of 52,382,872 imputed variants. The step-by-step variant quality control process is  
756 detailed in Supplementary Information section 1.  
757

### 758 Allele frequency trajectories

759 We computed allele frequency trajectories using all individuals in the time series. We used a  
760 moving average sliding window, with a window size of 1000 years and a step size of 100. We  
761 used a binomial likelihood function to estimate the mean, confidence intervals, and standard  
762 error. We smoothed the mean and standard error using the GaussianProcessRegressor  
763 function from the Scikit-learn library in Python. We parameterized this function with alpha =  
764 1e-4 and a 1\*RationalQuadratic kernel, with length\_scale\_bounds set to (10, 1e6). We  
765 clipped the resulting values to remain within the range of 0 and 1.  
766

767 **Assembly of GWAS data to which we correlated selection coefficients**

768 We processed 6,951 phenotypes with European ancestry from the Pan-UK Biobank<sup>24</sup>, of  
769 which 452 passed quality control with the flag phenotype\_qc\_EUR being PASS. We also  
770 analyzed 107 curated sets of independent GWAS studies<sup>55,217</sup> with European ancestry for  
771 meta-analysis. For the trans-ethnic analysis, we analyzed 31 phenotypes in East Asians: 30  
772 phenotypes from the Biobank of Japan (BBJ)<sup>218</sup> and the GWAS summary statistics from the  
773 study of years of schooling GWAS by Chen et al. 2024<sup>219</sup>. We then co-analyzed these GWAS  
774 results with that of the corresponding phenotypes in the Pan-UK Biobank.  
775  
776

777 **Data availability**  
778 The aligned sequences for newly reported data are available through the European Nucleotide  
779 Archive under an accession number that will be made available upon final publication.  
780 Imputed genomes for all ancient and modern individuals are available at the permanent  
781 Dataverse repository at a link that will be made available upon final publication.  
782

783 **Software and code availability**  
784 An interactive web application for this study is available at [https://reich-  
785 ages.rc.hms.harvard.edu](https://reich-ages.rc.hms.harvard.edu). The PQLseq2 software is available from  
786 <https://github.com/zhengli09/PQLseq2>.

787

788 **Acknowledgments**  
789 We thank Brian Browning, Shai Carmi, Evan Koch, Mark Lipson, Iain Mathieson, Vagheesh  
790 Narasimhan, Benjamin Neale, Simone Rubinacci, Guy Sella, and Shamil Sunyaev for  
791 discussions during the development of this project. We are grateful to Iosif Lazaridis, Heng  
792 Li, Adam Micco, Mariam Nawaz, Zhao Zhang, and Mengyao Zhao for bioinformatic support;  
793 and to Nicole Adamski, Rebecca Bernardos, Nasreen Broomandkhoshbacht, Kim Callan,  
794 Alex Claxton, Olivia Cheronet, Elizabeth Curtis, Matthew Ferry, Trudi Frost, Ilana  
795 Greenslade, Eadaoin Harney, Lora Iliev, Aisling Kearns, Jack Kellogg, Ann Marie Lawson,  
796 Megan Michel, Jonas Oppenheimer, Iris Patterson, Susanne Nordenfelt, Lijun Qiu, Kristin  
797 Stewardson, Anna Szécsényi-Nagy, Noah Workman and Fatma Zalzala for wet laboratory  
798 support. We are grateful to the archaeologists and anthropologists who supported early  
799 release of raw data for samples they shared with us for the purposes of studies of selection,  
800 decoupled from the archaeological contextual information which will be presented in papers  
801 on which they are co-authors and is necessary for any studies of the population history of  
802 these samples. This research was conducted by using the UK Biobank Resource under  
803 Application 16549. We acknowledge the Research Computing Group at Harvard Medical  
804 School, for their support with the computational analyses in this paper and the AGES web  
805 application; support from NIH grant HG012287; from the Allen Discovery Center program, a  
806 Paul G. Allen Frontiers Group advised program of the Paul G. Allen Family Foundation;  
807 from John Templeton Foundation grant 61220; and from the Howard Hughes Medical  
808 Institute (HHMI). This article is subject to HHMI's Open Access to Publications policy.  
809 HHMI lab heads have previously granted a nonexclusive CC BY 4.0 license to the public and  
810 a sublicensable license to HHMI in their research articles. Pursuant to those licenses, the  
811 author-accepted manuscript of this article can be made freely available under a CCBY 4.0  
812 license immediately upon publication.

## Tables

**Table 1. Re-evaluation of signals from five scans for selection in Holocene West Eurasia**

	Genome wide significant loci				Less stringent threshold			
	Total	Pass QC	$\pi>99\%$	$\pi>50\%$	Total	Pass QC	$\pi>99\%$	$\pi>50\%$
Mathieson et al. 2015	12	11	10	11				
Field et al. 2016	3	3	2	2	37	35	3	10
Le et al. 2022	24	22	9	10				
Kerner et al. 2023	3	3	3	3	139	123	14	24
Irving-Pease et al. 2024	21	21	13	17				

Note: Significance of selection according to our analysis for loci identified in five previous scans for selection in Holocene West Eurasia (all but Field et al. are ancient DNA-based scans). The less stringent P-value thresholds are  $10^{-5}$  for Field et al. 2016 and 0.05 for Kerner et al. 2023. The cumulative number of non-HLA signals identified as genome-wide significant and confirmed in our re-analysis with a posterior probability of selection  $\pi>99\%$  is 17 (6% of the 279 non-HLA loci with  $\pi>99\%$ ). Of these, 8 were found in Mathieson et al., Field et al. added 0, Le et al. added 3, Kerner et al. added 0, and Irving-Pease et al. added 6.

## Figure Legends

813 **Figure 1: Multiple lines of evidence show we are detecting genuine signals of directional  
814 selection. (a)** Proportion of SNPs significant in at least one of 452 Pan-UKBB GWAS, for  
815 SNPs with  $|X|$  above the value on the x-axis, and controlling for allele frequency. **(b)**  
816 Residual mean HAF-score  $[(HAF)/n]$ , computed as observed minus expected value, with n  
817 the haploid sample size, from a linear regression correcting for background selection, and a  
818 window size of 200 kb. **(c)** The heritability enrichment column is a meta-analysis on  
819 heritability enrichment for annotations based on a binary selection annotation, with FDR  
820 either below 1% (=1) or above 1% (=0). Z-score for change in selection intensity over time is  
821 based on a meta-analysis of heritability enrichment comparing key cultural transitions:  
822 Mesolithic-Neolithic (MN) to Bronze Age (BA); and Bronze Age (BA) to Historical Era  
823 (HE). We annotate each SNP according to whether it is among the top 5% with the highest  
824 probability of a stronger magnitude of selection coefficient in one time transect vs. another.  
825

826 **Figure 2: Genome scan for directional selection. (a)** The x-axis is chromosomal position,  
827 and the y-axis the selection signal for each variant. The dotted line indicates our genome-  
828 wide significance threshold of  $|X|=5.45$ . For clarity, only select loci are annotated. **(b)**  
829 Selection coefficient ( $s$ ) estimated from our scan plotted against minor allele frequency of  
830 tagging SNPs at independent loci with FDR<5%. Overlaid grids are simulation-based power  
831 estimates (90%, 70%, 50%, 30%, and 10% probability of detection). **(c)** The estimated age of  
832 the favored allele in a selective sweep versus the date of origin of the mutation is inferred  
833 from RELATE<sup>9</sup>, for tagging SNPs with FDR<5% at independent loci. The age of the sweep  
834 is defined as the time in the past when the frequency of the favored allele is expected to have  
835 been 0.0001 given the present-day frequency in 1000 Genomes Project European populations  
836 and assuming the selection coefficient has been constant over time.  
837

838 **Figure 3: Gallery of notable single-locus selection trajectories.** Each panel displays the  
839 derived allele frequency trajectory over time for a variant (uncorrected for structure), along  
840 with selection coefficient ( $s$ ), selection statistic ( $X$ ), and posterior probability of selection ( $\pi$ ).  
841 Circles represent frequencies in Western Hunter-Gatherers (orange), Early European Farmers  
842 (green), and Steppe Pastoralists (blue). The highlighted loci are not necessarily those with the  
843 strongest signals, and even include negative results. We highlight them here because of their  
844 biological interest and because they speak to long-standing debates. For Panels 4, 5, 6, 33, 35,  
845 and 36 separate analyses are shown for transects before and after a manually selected peak  
846 (marked by a black line), with 200-year overlap. In cases where  $\pi>90\%$ , the confidence  
847 interval is shaded blue (or blue for before and red for after the split); otherwise, the shading is  
848 gray. Variants reported in other ancient DNA studies are marked with an asterisk.  
849

850 **Figure 4: Coordinated selection on alleles affecting same traits (polygenic adaptation).**  
851 The polygenic score of Western Eurasians over 14000 years in black, with 95% confidence  
852 interval in gray. Red represents the linear mixed model regression, adjusted for population  
853 structure, with slope  $\gamma$ . Three tests of polygenic selection— $\gamma$ ,  $\gamma_{sign}$ , and  $r_s$ —are all significant  
854 for each of these twelve traits, with the relevant statistics at the top of each panel.

## Extended Data Figure Legends

- 855 **Extended Data Figure 1: Spatiotemporal distribution of individuals and effect on power.**  
856 **(a)** Geographic origin: North (N), Central (C), East (E), Southwest (SW) and Southeast (SE).  
857 **(b)** Temporal distribution (x-axis on a logarithmic scale). **(c)** Power analysis based on  
858 simulations. Sample size, dates, and pattern of genetic relatedness are matched to real data.  
859 Power is defined as proportion of true positives expected at  $p < 5 \times 10^{-8}$ . We ran 20000  
860 simulations for each selection coefficient, with minor allele frequency (MAF) at present  
861 (time=0) randomly drawn from the MAF distribution in modern Europeans. **(d)** Number of  
862 independent and significant loci as function of sample size (from downsampling). **(e)** Effect  
863 of age on power. Data are divided into 10 non-overlapping periods; modern individuals are a  
864 separate bin. In top panel, y-axis is proportion of loci that remain significant after excluding  
865 100 random individuals from that bin (bottom is number of individuals in the same bin).  
866
- 867 **Extended Data Figure 2: High proportion of genome affected by directional selection.**  
868 **(a)** LD score plot for nominal  $\chi^2$  statistics, with each point representing an LD score quantile.  
869 Values are averaged across each bin. **(b)** Mapping X-score to posterior probability ( $\pi$ ), False  
870 Discovery Rate (FDR), number of independent loci excluding the HLA region (N), and the  
871 percentage of the genome in LD ( $r^2 > 0.05$ ) with tag SNPs representing these loci.  
872
- 873 **Extended Data Figure 3: Robustness of directional selection signals (related to Figure**  
874 **1a,b).** **(a)** Proportion of SNPs significant in any of 452 pan-UK Biobank GWAS studies for  
875 X-statistics with magnitudes larger than the threshold on the x-axis, adjusted for minor allele  
876 frequency and measures of linked purifying selection (McVicker-B, Murphy-phastCons, and  
877 Murphy-CADD). Background selection tends to be higher in functional genomic regions, so  
878 SNPs with higher  $|X|$  are more penalized than in Figure 1a hence the lower plateau. **(b)**  
879 Simulating neutral, negative, and positive selection for a 200 kb window around a focal SNP,  
880 with derived allele frequency drawn uniformly from [0,1]. The focal SNP has  $s=0.01$ ,  
881 population size is constant at 20000 diploid individuals, mutation rate per base pair per  
882 generation is  $2 \times 10^{-8}$ , and recombination rate is 1 cM per 1 Mb. **(c)** Residual mean (HAF)/n  
883 for a haploid sample size n over 200 bp windows is observed minus expected value. Expected  
884 value is determined using a linear regression model with McVicker-B, Murphy-phastCons,  
885 and Murphy-CADD as variables, providing the expected mean (HAF)/n conditioned on them.  
886
- 887 **Extended Data Figure 4: Stratified LD Score Regression shows that alleles affecting**  
888 **blood-immune-inflammatory and cardio-metabolic traits were unusually affected by**  
889 **selection, and that selection intensity increased in the Bronze Age (related to Figure 1c).**  
890 **(a)** We annotated sites based on their inferred strength of selection—based on their FDR  
891 being above a specified threshold, or 1-FDR as a continuous annotation—and used Stratified  
892 LD Score Regression (S-LDSC) to study enrichment of GWAS signals and standardized  
893 effect sizes ( $\tau^*$ ) for traits in different functional categories. Our analysis adjusts for 97  
894 annotations that are known to affect heritability and are part of the standard correction in S-  
895 LDSC; dots represent significance of elevation above the baseline of 1 expected for random  
896 variants. **(b)** Tests for changes in selection intensity during different cultural transitions:  
897 Mesolithic-Neolithic (MN) to Bronze Age (BA); and Bronze Age (BA) to Historical Era  
898 (HE). Each annotation is binary, identifying SNPs among the top 5% with the highest  
899 probability of experiencing stronger selection during one time period compared to another.  
900 This is determined using the estimated selection coefficient and standard error from models  
901 separately fit to each cultural period. Error bars are 95% confidence intervals.

902

**Extended Data Figure 5: How selection coefficients on single variants changed in intensity over time (for the gallery of 36 loci also highlighted in Figure 3).** Time-variant selection coefficients are estimated by refitting our model in sliding windows of 2000 years, with a step size of 100 years, and a minimum of 500 people per window. The present-day is excluded. Color map represents the Z-score for the selection coefficient being non-zero in that window, ranging from -5 (dark red) to 5 (dark blue).

909

**Extended Data Figure 6: Genotype-phenotype correlations for the signals of selection for Celiac disease at HLA and the ABO blood group locus.** (a) Prevalence and (b) prevalence ratio of individuals with celiac disease or gluten sensitivity (data field 21068) in the UK Biobank, conditioned on the genotype of rs3891176 (C>A). The prevalence ratio compared to the A/A genotype as a baseline; bars are 95% confidence intervals. (c) Left: Blood type frequency trajectories for O, A, B, and AB estimated from our aDNA time series. Right: Genealogy of the ABO alleles approximated by Shelton et al. 2021<sup>220</sup>. The allele frequencies are estimated from Europeans in the 1000 Genomes Project; shading gives 95% confidence interval. (d) Significant association to traits in Pan-UKBB for the two base pair insertion rs8176719 (T>TC) and SNP rs8176746 (G>T), approximating the alleles A and B.

920

**Extended Data Figure 7: High correlation of 3 tests for polygenic selection ( $\gamma$ ,  $\gamma_{\text{sign}}$ ,  $r_s$ ).** Each dot represents a phenotype, some annotated by colors. Pearson's correlation for x and y axes at top; dashed line is the P<0.0001 significance threshold (correcting for 500 tests).

924

**Extended Data Figure 8: How coordinated selection on alleles affecting the same traits changed in intensity over time (gallery of 12 complex traits also highlighted in Figure 4).** We estimate time-variant polygenic selection intensity  $\gamma$  by refitting our model in sliding windows of 2000 years, with a step size of 100 years, and a minimum of 500 people per window. The present-day is excluded. Color map represents the Z-score for the selection coefficient being non-zero in that window, ranging from -5 (dark red) to 5 (dark blue).

931

**Extended Data Figure 9: Pigmentation is oligogenic but selection on it was polygenic.** Selection coefficient ( $s$ ) and effect size ( $\beta$ ) from the pan-UKBB skin color phenotype for 110 independent SNPs passing the GWAS P-value threshold of  $p < 5 \times 10^{-8}$ . Following <sup>57</sup>, the orange line is a linear regression on all SNPs (99 blue and 11 orange markers), while the blue line includes only SNPs with  $|\beta| < 0.05$  (99 blue markers). Although the correlation appears different (with the difference between Fisher Z-transformed Pearson r showing a P-value of 0.001), the slopes are not significantly different ( $P = 0.10$ ), consistent with a model in which selection for pigmentation had an equal impact on all variants in proportion to effect size.

940

**Extended Data Figure 10: Estimating the minimum number of SNPs affected by selection for each trait (gallery of 12 traits also highlighted in Figure 4).** Each panel shows the correlation of a trait with selection summary statistics ( $r_s$ ) as a function of number of dropped loci. The right axis displays  $r_s$  in blue; P-value on the left axis in orange. For each SNP, we define a priority score  $|\beta \times s \times f \times (1-f)|$ , where  $\beta$  is the GWAS effect size,  $s$  the selection coefficient, and  $f$  allele frequency. SNPs are sorted by priority score, and in each iteration, a 2cM region around the highest priority SNP is dropped,  $r_s$  is recalculated for the remaining genome, and this continues until no SNPs are left. (b) We similarly show  $\gamma$  estimates at right as a function of number of dropped SNPs (blue), and P-value for polygenic selection at left with dark orange P<0.0001, light orange P<0.05, and gray otherwise.

951

952 **Extended Data Figure 11: Replication of signals of polygenic selection using effect size**  
953 **estimates in East Asians whose population structure is uncorrelated to West Eurasians.**  
954 We applied our polygenic selection test to 31 traits using pairs of GWAS studies for the trait,  
955 one from Europe and one from East Asia. We assessed if PGS ( $\gamma$ ), PGS-sign ( $\gamma_{\text{sign}}$ ), and  
956 genetic correlation tests ( $r_s$ ) were consistent in these two analyses.  
957

958 **Extended Data Figure 12: Correlations of polygenic scores for complex traits with**  
959 **strong evidence of coordinated selection (the same 12 traits highlighted in Figure 4).**  
960 Genetic correlations of traits were computed using LDSC. Asterisks indicate significance  
961 level (n asterisks represent a jackknife estimated  $P < 0.5 \times 10^{-n}$ ).  
962

963 **Extended Data Figure 13: Consistency of polygenic selection signals using effect sizes**  
964 **estimated from both GWAS of unrelated people, and sibling-based GWAS<sup>66</sup>.** The first  
965 three columns show estimates for each of the three polygenic tests of selection. The fourth  
966 column replicates Figure 5 from<sup>66</sup>, and shows the estimated SNP heritability  $h^2$  by LDSC.  
967 The fifth column shows the sample sizes for both GWAS of unrelated people (blue) and  
968 sibling-based GWAS (orange). Error bars indicate the 95% confidence interval, which is  
969 often larger for the sibling-based GWAS due to limited sample size.  
970

971 **Extended Data Figure 14: Our generalized linear mixed model (GLMM) method is far**  
972 **more powerful than a generalized linear model (GLM) with PC covariates.** To compute  
973 the inflation factor for different approaches, we ran 10000 simulations of neutral evolution  
974 for a scenario of population structure, sample size, and temporal distribution of samples  
975 matching real data. For the power calculation, we ran 20000 simulations of selective sweeps  
976 for a range of selection coefficients (power is the proportion of true positives at  $P < 5 \times 10^{-8}$ ).  
977 Because of co-linearity of time and population structure, correcting for PCs greatly weakens  
978 power to detect selection, but the GLMM methodology does not suffer from this.

## Supplementary Data Sets

- 979 **Online Table 1: List of 8433 ancient individuals analyzed in our time transect.** Data  
980 Source 1 is 3644 individuals whose previously published sequences we reanalyze. Data  
981 Source 2 is 244 individuals with previously published in-solution enrichment data for which  
982 we report and analyze whole genome shotgun data. Data Source 3 is 74 individuals with  
983 previously published in-solution enrichment data for which we report and analyze additional  
984 in-solution enrichment data. Data Source 4 is 4471 never-before-reported individuals for  
985 which we report and analyze data that is anonymized except for a point estimate of the data  
986 of origin and information about broad region in West Eurasia. Available as an Excel table.  
987
- 988 **Online Table 2: List of 300 newly reported shotgun ancient genomes.** Most are from  
989 individuals with previously reported in-solution enrichment data (n=244; the remainder are  
990 from samples reported for the first time (n=56). Available as an Excel table.  
991
- 992 **Online Table 3: List of 5382 newly reported ancient DNA libraries.** The majority  
993 (n=5227) are from 4471 never-before-reported ancient individuals; the rest (n=155) are from  
994 74 individuals for which we increase data quality. Available as an Excel table.  
995
- 996 **Online Table 4: Summary statistics for selection in 9.9 million variants.** The data are  
997 provided as a tab-delimited text file, compressed using gzip. Available at Harvard Dataverse:  
998 <https://doi.org/10.7910/DVN/7RVV9N>.  
999
- 1000 **Online Table 5: Summary statistics for tests of polygenic selection.** The data includes: 452  
1001 European GWAS from Pan-UKBB<sup>24</sup>, 107 curated European GWAS used for S-LDSC meta-  
1002 analysis<sup>55,217</sup>, 50 European GWAS with 25 pairs of sibling and population GWAS from Howe  
1003 et al. 2022<sup>66</sup>, 30 East Asian GWAS from Biobank Japan, and one from Chen et al. 2024<sup>219</sup>.  
1004 Available as an Excel table.

## References

1. Racimo, F., Sikora, M., Vander Linden, M., Schroeder, H. & Lalueza-Fox, C. Beyond broad strokes: sociocultural insights from the study of ancient genomes. *Nat. Rev. Genet.* **21**, 355–366 (2020).
2. Kerner, G., Choin, J. & Quintana-Murci, L. Ancient DNA as a tool for medical research. *Nat. Med.* **29**, 1048–1051 (2023).
3. Bennett, E. A. & Fu, Q. Ancient genomes and the evolutionary path of modern humans. *Cell* **187**, 1042–1046 (2024).
4. Chen, H., Patterson, N. & Reich, D. Population differentiation as a test for selective sweeps. *Genome Res.* **20**, 393–402 (2010).
5. Yi, X. *et al.* Sequencing of 50 human exomes reveals adaptation to high altitude. *Science* **329**, 75–78 (2010).
6. Sabeti, P. C. *et al.* Detecting recent positive selection in the human genome from haplotype structure. *Nature* **419**, 832–837 (2002).
7. Voight, B. F., Kudaravalli, S., Wen, X. & Pritchard, J. K. A map of recent positive selection in the human genome. *PLoS Biol.* **4**, e72 (2006).
8. Field, Y. *et al.* Detection of human adaptation during the past 2000 years. *Science* **354**, 760–764 (2016).
9. Speidel, L., Forest, M., Shi, S. & Myers, S. R. A method for genome-wide genealogy estimation for thousands of samples. *Nat. Genet.* **51**, 1321–1329 (2019).
10. Berg, J. J. & Coop, G. A Coalescent Model for a Sweep of a Unique Standing Variant. *Genetics* **201**, 707–725 (2015).
11. Mathieson, I. *et al.* Genome-wide patterns of selection in 230 ancient Eurasians. *Nature* **528**, 499–503 (2015).
12. Le, M. K. *et al.* 1,000 ancient genomes uncover 10,000 years of natural selection in Europe. *BioRxiv Prepr. Serv. Biol.* 2022.08.24.505188 (2022) doi:10.1101/2022.08.24.505188.
13. Kerner, G. *et al.* Genetic adaptation to pathogens and increased risk of inflammatory disorders in post-Neolithic Europe. *Cell Genomics* **3**, 100248 (2023).
14. Irving-Pease, E. K. *et al.* The selection landscape and genetic legacy of ancient Eurasians. *Nature* **625**, 312–320 (2024).
15. Pritchard, J. K., Pickrell, J. K. & Coop, G. The genetics of human adaptation: hard sweeps, soft sweeps, and polygenic adaptation. *Curr. Biol. CB* **20**, R208-215 (2010).
16. Gao, Z. Unveiling recent and ongoing adaptive selection in human populations. *PLoS Biol.* **22**, e3002469 (2024).
17. Mallick, S. *et al.* The Allen Ancient DNA Resource (AADR) a curated compendium of ancient human genomes. *Sci. Data* **11**, 182 (2024).
18. Byrska-Bishop, M. *et al.* High-coverage whole-genome sequencing of the expanded 1000 Genomes Project cohort including 602 trios. *Cell* **185**, 3426-3440.e19 (2022).
19. Bycroft, C. *et al.* The UK Biobank resource with deep phenotyping and genomic data. *Nature* **562**, 203–209 (2018).
20. Rubinacci, S., Ribeiro, D. M., Hofmeister, R. J. & Delaneau, O. Efficient phasing and imputation of low-coverage sequencing data using large reference panels. *Nat. Genet.* **53**, 120–126 (2021).
21. Yang, J. *et al.* Genomic inflation factors under polygenic inheritance. *Eur. J. Hum. Genet. EJHG* **19**, 807–812 (2011).
22. Devlin, B., Roeder, K. & Wasserman, L. Genomic control, a new approach to genetic-based association studies. *Theor. Popul. Biol.* **60**, 155–166 (2001).

23. Bulik-Sullivan, B. K. *et al.* LD Score regression distinguishes confounding from polygenicity in genome-wide association studies. *Nat. Genet.* **47**, 291–295 (2015).
24. Karczewski, K. J. *et al.* Pan-UK Biobank GWAS improves discovery, analysis of genetic architecture, and resolution into ancestry-enriched effects. 2024.03.13.24303864 Preprint at <https://doi.org/10.1101/2024.03.13.24303864> (2024).
25. Ronen, R. *et al.* Predicting Carriers of Ongoing Selective Sweeps without Knowledge of the Favored Allele. *PLoS Genet.* **11**, e1005527 (2015).
26. Akbari, A. *et al.* Identifying the Favored Mutation in a Positive Selective Sweep. *Nat. Methods* **15**, 279–282 (2018).
27. McVicker, G., Gordon, D., Davis, C. & Green, P. Widespread genomic signatures of natural selection in hominid evolution. *PLoS Genet.* **5**, e1000471 (2009).
28. Murphy, D. A., Elyashiv, E., Amster, G. & Sella, G. Broad-scale variation in human genetic diversity levels is predicted by purifying selection on coding and non-coding elements. *eLife* **12**, e76065 (2023).
29. Finucane, H. K. *et al.* Partitioning heritability by functional annotation using genome-wide association summary statistics. *Nat. Genet.* **47**, 1228–1235 (2015).
30. Abadie, V., Sollid, L. M., Barreiro, L. B. & Jabri, B. Integration of genetic and immunological insights into a model of celiac disease pathogenesis. *Annu. Rev. Immunol.* **29**, 493–525 (2011).
31. Sams, A. & Hawks, J. Patterns of population differentiation and natural selection on the celiac disease background risk network. *PloS One* **8**, e70564 (2013).
32. Sams, A. & Hawks, J. Celiac disease as a model for the evolution of multifactorial disease in humans. *Hum. Biol.* **86**, 19–36 (2014).
33. Abegaz, S. B. Human ABO Blood Groups and Their Associations with Different Diseases. *BioMed Res. Int.* **2021**, 6629060 (2021).
34. Pettenkofer, H. J., Stoess, B., Helmbold, W. & Vogel, F. Alleged causes of the present-day world distribution of the human ABO blood groups. *Nature* **193**, 445–446 (1962).
35. Medland, S. E. *et al.* Common Variants in the Trichohyalin Gene Are Associated with Straight Hair in Europeans. *Am. J. Hum. Genet.* **85**, 750–755 (2009).
36. Kerner, G. *et al.* Homozygosity for TYK2 P1104A underlies tuberculosis in about 1% of patients in a cohort of European ancestry. *Proc. Natl. Acad. Sci. U. S. A.* **116**, 10430–10434 (2019).
37. Kerner, G. *et al.* Human ancient DNA analyses reveal the high burden of tuberculosis in Europeans over the last 2,000 years. *Am. J. Hum. Genet.* **108**, 517–524 (2021).
38. Barrie, W. *et al.* Elevated genetic risk for multiple sclerosis emerged in steppe pastoralist populations. *Nature* **625**, 321–328 (2024).
39. Moutsianas, L. *et al.* Class II HLA interactions modulate genetic risk for multiple sclerosis. *Nat. Genet.* **47**, 1107–1113 (2015).
40. Moalem, S., Percy, M. E., Kruck, T. P. A. & Gelbart, R. R. Epidemic pathogenic selection: an explanation for hereditary hemochromatosis? *Med. Hypotheses* **59**, 325–329 (2002).
41. Bos, K. I. *et al.* A draft genome of Yersinia pestis from victims of the Black Death. *Nature* **478**, 506–510 (2011).
42. Wagner, D. M. *et al.* Yersinia pestis and the plague of Justinian 541–543 AD: a genomic analysis. *Lancet Infect. Dis.* **14**, 319–326 (2014).
43. Samson, M. *et al.* Resistance to HIV-1 infection in caucasian individuals bearing mutant alleles of the CCR-5 chemokine receptor gene. *Nature* **382**, 722–725 (1996).
44. Hütter, G. *et al.* Long-term control of HIV by CCR5 Delta32/Delta32 stem-cell transplantation. *N. Engl. J. Med.* **360**, 692–698 (2009).

45. Gupta, R. K. *et al.* HIV-1 remission following CCR5 $\Delta$ 32/ $\Delta$ 32 haematopoietic stem-cell transplantation. *Nature* **568**, 244–248 (2019).
46. Stephens, J. C. *et al.* Dating the origin of the CCR5-Delta32 AIDS-resistance allele by the coalescence of haplotypes. *Am. J. Hum. Genet.* **62**, 1507–1515 (1998).
47. Novembre, J., Galvani, A. P. & Slatkin, M. The geographic spread of the CCR5 Delta32 HIV-resistance allele. *PLoS Biol.* **3**, e339 (2005).
48. Sabeti, P. C. *et al.* The Case for Selection at CCR5- $\Delta$ 32. *PLoS Biol.* **3**, e378 (2005).
49. Seersholm, F. V. *et al.* Repeated plague infections across six generations of Neolithic Farmers. *Nature* 1–8 (2024) doi:10.1038/s41586-024-07651-2.
50. Rasmussen, S. *et al.* Early divergent strains of Yersinia pestis in Eurasia 5,000 years ago. *Cell* **163**, 571–582 (2015).
51. Spyrou, M. A. *et al.* Analysis of 3800-year-old Yersinia pestis genomes suggests Bronze Age origin for bubonic plague. *Nat. Commun.* **9**, 2234 (2018).
52. Kerem, B. *et al.* Identification of the cystic fibrosis gene: genetic analysis. *Science* **245**, 1073–1080 (1989).
53. Cutting, G. R. Cystic fibrosis genetics: from molecular understanding to clinical application. *Nat. Rev. Genet.* **16**, 45–56 (2015).
54. Gabriel, S. E., Brigman, K. N., Koller, B. H., Boucher, R. C. & Stutts, M. J. Cystic fibrosis heterozygote resistance to cholera toxin in the cystic fibrosis mouse model. *Science* **266**, 107–109 (1994).
55. Kim, A. *et al.* Inferring causal cell types of human diseases and risk variants from candidate regulatory elements. 2024.05.17.24307556 Preprint at <https://doi.org/10.1101/2024.05.17.24307556> (2024).
56. Chen, M. *et al.* Evidence of Polygenic Adaptation in Sardinia at Height-Associated Loci Ascertained from the Biobank Japan. *Am. J. Hum. Genet.* **107**, 60–71 (2020).
57. Ju, D. & Mathieson, I. The evolution of skin pigmentation-associated variation in West Eurasia. *Proc. Natl. Acad. Sci. U. S. A.* **118**, e2009227118 (2021).
58. Ding, Y. *et al.* Polygenic scoring accuracy varies across the genetic ancestry continuum. *Nature* **618**, 774–781 (2023).
59. Bulik-Sullivan, B. *et al.* An atlas of genetic correlations across human diseases and traits. *Nat. Genet.* **47**, 1236–1241 (2015).
60. Berg, J. J. *et al.* Reduced signal for polygenic adaptation of height in UK Biobank. *eLife* **8**, e39725 (2019).
61. Sohail, M. *et al.* Polygenic adaptation on height is overestimated due to uncorrected stratification in genome-wide association studies. *eLife* **8**, e39702 (2019).
62. O'Connor, L. J. *et al.* Extreme Polygenicity of Complex Traits Is Explained by Negative Selection. *Am. J. Hum. Genet.* **105**, 456–476 (2019).
63. Beauchamp, J. P. Genetic evidence for natural selection in humans in the contemporary United States. *Proc. Natl. Acad. Sci. U. S. A.* **113**, 7774–7779 (2016).
64. Kong, A. *et al.* Selection against variants in the genome associated with educational attainment. *Proc. Natl. Acad. Sci. U. S. A.* **114**, E727–E732 (2017).
65. Sanjak, J. S., Sidorenko, J., Robinson, M. R., Thornton, K. R. & Visscher, P. M. Evidence of directional and stabilizing selection in contemporary humans. *Proc. Natl. Acad. Sci. U. S. A.* **115**, 151–156 (2018).
66. Howe, L. J. *et al.* Within-sibship genome-wide association analyses decrease bias in estimates of direct genetic effects. *Nat. Genet.* **54**, 581–592 (2022).
67. Hernandez, R. D. *et al.* Classic selective sweeps were rare in recent human evolution. *Science* **331**, 920–924 (2011).
68. Coop, G. *et al.* The role of geography in human adaptation. *PLoS Genet.* **5**, e1000500 (2009).

69. Simon, A. & Coop, G. The contribution of gene flow, selection, and genetic drift to five thousand years of human allele frequency change. *bioRxiv* 2023.07.11.548607 (2024) doi:10.1101/2023.07.11.548607.
70. Koch, E. *et al.* Genetic association data are broadly consistent with stabilizing selection shaping human common diseases and traits. 2024.06.19.599789 Preprint at <https://doi.org/10.1101/2024.06.19.599789> (2024).
71. Yang, J., Zaitlen, N. A., Goddard, M. E., Visscher, P. M. & Price, A. L. Advantages and pitfalls in the application of mixed-model association methods. *Nat. Genet.* **46**, 100–106 (2014).
72. Taus, T., Futschik, A. & Schlötterer, C. Quantifying Selection with Pool-Seq Time Series Data. *Mol. Biol. Evol.* **34**, 3023–3034 (2017).
73. Crow, J. F. *An Introduction to Population Genetics Theory*. (Scientific Publishers, 2017).
74. Sun, S. *et al.* Heritability estimation and differential analysis of count data with generalized linear mixed models in genomic sequencing studies. *Bioinforma. Oxf. Engl.* **35**, 487–496 (2019).
75. Loh, P.-R. *et al.* Efficient Bayesian mixed model analysis increases association power in large cohorts. *Nat. Genet.* **47**, 284–290 (2015).
76. Listgarten, J. *et al.* Improved linear mixed models for genome-wide association studies. *Nat. Methods* **9**, 525–526 (2012).
77. Zhou, X. & Stephens, M. Genome-wide efficient mixed-model analysis for association studies. *Nat. Genet.* **44**, 821–824 (2012).
78. Shi, H. *et al.* Population-specific causal disease effect sizes in functionally important regions impacted by selection. *Nat. Commun.* **12**, 1098 (2021).
79. Gazal, S. *et al.* Linkage disequilibrium-dependent architecture of human complex traits shows action of negative selection. *Nat. Genet.* **49**, 1421–1427 (2017).
80. Gazal, S., Marquez-Luna, C., Finucane, H. K. & Price, A. L. Reconciling S-LDSC and LDAK functional enrichment estimates. *Nat. Genet.* **51**, 1202–1204 (2019).
81. Damgaard, P. D. B. *et al.* 137 ancient human genomes from across the Eurasian steppes. *Nature* **557**, 369–374 (2018).
82. Jensen, T. Z. T. *et al.* A 5700 year-old human genome and oral microbiome from chewed birch pitch. *Nat. Commun.* **10**, 5520 (2019).
83. Olalde, I. *et al.* A Common Genetic Origin for Early Farmers from Mediterranean Cardial and Central European LBK Cultures. *Mol. Biol. Evol.* msv181 (2015) doi:10.1093/molbev/msv181.
84. Cassidy, L. M. *et al.* A dynastic elite in monumental Neolithic society. *Nature* **582**, 384–388 (2020).
85. Moots, H. M. *et al.* A genetic history of continuity and mobility in the Iron Age central Mediterranean. *Nat. Ecol. Evol.* **7**, 1515–1524 (2023).
86. Olalde, I. *et al.* A genetic history of the Balkans from Roman frontier to Slavic migrations. *Cell* **186**, 5472-5485.e9 (2023).
87. Nikitin, A. G. *et al.* A genomic history of the North Pontic Region from the Neolithic to the Bronze Age. Preprint at <https://doi.org/10.1101/2024.04.17.589600> (2024).
88. Fernandes, D. M. *et al.* A genomic Neolithic time transect of hunter-farmer admixture in central Poland. *Sci. Rep.* **8**, 14879 (2018).
89. Fowler, C. *et al.* A high-resolution picture of kinship practices in an Early Neolithic tomb. *Nature* **601**, 584–587 (2022).
90. Harney, É. *et al.* A minimally destructive protocol for DNA extraction from ancient teeth. *Genome Res.* **31**, 472–483 (2021).

91. González-Fortes, G. *et al.* A western route of prehistoric human migration from Africa into the Iberian Peninsula. *Proc. R. Soc. B Biol. Sci.* **286**, 20182288 (2019).
92. Marciak, S. *et al.* An integrative skeletal and paleogenomic analysis of stature variation suggests relatively reduced health for early European farmers. *Proc. Natl. Acad. Sci.* **119**, e2106743119 (2022).
93. Unterländer, M. *et al.* Ancestry and demography and descendants of Iron Age nomads of the Eurasian Steppe. *Nat. Commun.* **8**, 14615 (2017).
94. Dulias, K. *et al.* Ancient DNA at the edge of the world: Continental immigration and the persistence of Neolithic male lineages in Bronze Age Orkney. *Proc. Natl. Acad. Sci.* **119**, e2108001119 (2022).
95. Zalloua, P. *et al.* Ancient DNA of Phoenician remains indicates discontinuity in the settlement history of Ibiza. *Sci. Rep.* **8**, 17567 (2018).
96. Skourtanioti, E. *et al.* Ancient DNA reveals admixture history and endogamy in the prehistoric Aegean. *Nat. Ecol. Evol.* **7**, 290–303 (2023).
97. Lamnidis, T. C. *et al.* Ancient Fennoscandian genomes reveal origin and spread of Siberian ancestry in Europe. *Nat. Commun.* **9**, 5018 (2018).
98. O’Sullivan, N. *et al.* Ancient genome-wide analyses infer kinship structure in an Early Medieval Alemannic graveyard. *Sci. Adv.* **4**, eaao1262 (2018).
99. Rivollat, M. *et al.* Ancient genome-wide DNA from France highlights the complexity of interactions between Mesolithic hunter-gatherers and Neolithic farmers. *Sci. Adv.* **6**, eaaz5344 (2020).
100. Ebenesersdóttir, S. S. *et al.* Ancient genomes from Iceland reveal the making of a human population. *Science* **360**, 1028–1032 (2018).
101. Fregel, R. *et al.* Ancient genomes from North Africa evidence prehistoric migrations to the Maghreb from both the Levant and Europe. *Proc. Natl. Acad. Sci.* **115**, 6774–6779 (2018).
102. Brunel, S. *et al.* Ancient genomes from present-day France unveil 7,000 years of its demographic history. *Proc. Natl. Acad. Sci.* **117**, 12791–12798 (2020).
103. Brace, S. *et al.* Ancient genomes indicate population replacement in Early Neolithic Britain. *Nat. Ecol. Evol.* **3**, 765–771 (2019).
104. Günther, T. *et al.* Ancient genomes link early farmers from Atapuerca in Spain to modern-day Basques. *Proc. Natl. Acad. Sci.* **112**, 11917–11922 (2015).
105. Žegarac, A. *et al.* Ancient genomes provide insights into family structure and the heredity of social status in the early Bronze Age of southeastern Europe. *Sci. Rep.* **11**, 10072 (2021).
106. Gnechi-Ruscone, G. A. *et al.* Ancient genomes reveal origin and rapid trans-Eurasian migration of 7th century Avar elites. *Cell* **185**, 1402-1413.e21 (2022).
107. Saupe, T. *et al.* Ancient genomes reveal structural shifts after the arrival of Steppe-related ancestry in the Italian Peninsula. *Curr. Biol.* **31**, 2576-2591.e12 (2021).
108. Sikora, M. *et al.* Ancient genomes show social and reproductive behavior of early Upper Paleolithic foragers. *Science* **358**, 659–662 (2017).
109. Krzewińska, M. *et al.* Ancient genomes suggest the eastern Pontic-Caspian steppe as the source of western Iron Age nomads. *Sci. Adv.* **4**, eaat4457 (2018).
110. Gnechi-Ruscone, G. A. *et al.* Ancient genomic time transect from the Central Asian Steppe unravels the history of the Scythians. *Sci. Adv.* **7**, eabe4414 (2021).
111. Wang, C.-C. *et al.* Ancient human genome-wide data from a 3000-year interval in the Caucasus corresponds with eco-geographic regions. *Nat. Commun.* **10**, 590 (2019).
112. Lazaridis, I. *et al.* Ancient human genomes suggest three ancestral populations for present-day Europeans. *Nature* **513**, 409–413 (2014).

113. Ariano, B. *et al.* Ancient Maltese genomes and the genetic geography of Neolithic Europe. *Curr. Biol.* **32**, 2668-2680.e6 (2022).
114. Antonio, M. L. *et al.* Ancient Rome: A genetic crossroads of Europe and the Mediterranean. *Science* **366**, 708–714 (2019).
115. Scorrano, G. *et al.* Bioarchaeological and palaeogenomic portrait of two Pompeians that died during the eruption of Vesuvius in 79 AD. *Sci. Rep.* **12**, 6468 (2022).
116. Srigyan, M. *et al.* Bioarchaeological evidence of one of the earliest Islamic burials in the Levant. *Commun. Biol.* **5**, 554 (2022).
117. Furtwängler, A. *et al.* Comparison of Target Enrichment Strategies for Ancient Pathogen DNA. *BioTechniques* **69**, 455–459 (2020).
118. Linderholm, A. *et al.* Corded Ware cultural complexity uncovered using genomic and isotopic analysis from south-eastern Poland. *Sci. Rep.* **10**, 6885 (2020).
119. Gokhman, D. *et al.* Differential DNA methylation of vocal and facial anatomy genes in modern humans. *Nat. Commun.* **11**, 1189 (2020).
120. Papac, L. *et al.* Dynamic changes in genomic and social structures in third millennium BCE central Europe. *Sci. Adv.* **7**, eabi6941 (2021).
121. Hofmanová, Z. *et al.* Early farmers from across Europe directly descended from Neolithic Aegeans. *Proc. Natl. Acad. Sci.* **113**, 6886–6891 (2016).
122. Broushaki, F. *et al.* Early Neolithic genomes from the eastern Fertile Crescent. *Science* **353**, 499–503 (2016).
123. Scheib, C. L. *et al.* East Anglian early Neolithic monument burial linked to contemporary Megaliths. *Ann. Hum. Biol.* **46**, 145–149 (2019).
124. Saag, L. *et al.* Extensive Farming in Estonia Started through a Sex-Biased Migration from the Steppe. *Curr. Biol.* **27**, 2185-2193.e6 (2017).
125. Valdiosera, C. *et al.* Four millennia of Iberian biomolecular prehistory illustrate the impact of prehistoric migrations at the far end of Eurasia. *Proc. Natl. Acad. Sci.* **115**, 3428–3433 (2018).
126. Peltola, S. *et al.* Genetic admixture and language shift in the medieval Volga-Oka interfluve. *Curr. Biol.* **33**, 174-182.e10 (2023).
127. Saag, L. *et al.* Genetic ancestry changes in Stone to Bronze Age transition in the East European plain. *Sci. Adv.* **7**, eabd6535 (2021).
128. Marcus, J. H. *et al.* Genetic history from the Middle Neolithic to present on the Mediterranean island of Sardinia. *Nat. Commun.* **11**, 939 (2020).
129. Lazaridis, I. *et al.* Genetic origins of the Minoans and Mycenaeans. *Nature* **548**, 214–218 (2017).
130. Gamba, C. *et al.* Genome flux and stasis in a five millennium transect of European prehistory. *Nat. Commun.* **5**, 5257 (2014).
131. Novak, M. *et al.* Genome-wide analysis of nearly all the victims of a 6200 year old massacre. *PLOS ONE* **16**, e0247332 (2021).
132. Waldman, S. *et al.* Genome-wide data from medieval German Jews show that the Ashkenazi founder event pre-dated the 14th century. *Cell* **185**, 4703-4716.e16 (2022).
133. Immel, A. *et al.* Genome-wide study of a Neolithic Wartberg grave community reveals distinct HLA variation and hunter-gatherer ancestry. *Commun. Biol.* **4**, 113 (2021).
134. Brace, S. *et al.* Genomes from a medieval mass burial show Ashkenazi-associated hereditary diseases pre-date the 12th century. *Curr. Biol.* **32**, 4350-4359.e6 (2022).
135. Gelabert, P. *et al.* Genomes from Verteba cave suggest diversity within the Trypillians in Ukraine. *Sci. Rep.* **12**, 7242 (2022).
136. Yu, H. *et al.* Genomic and dietary discontinuities during the Mesolithic and Neolithic in Sicily. *iScience* **25**, 104244 (2022).

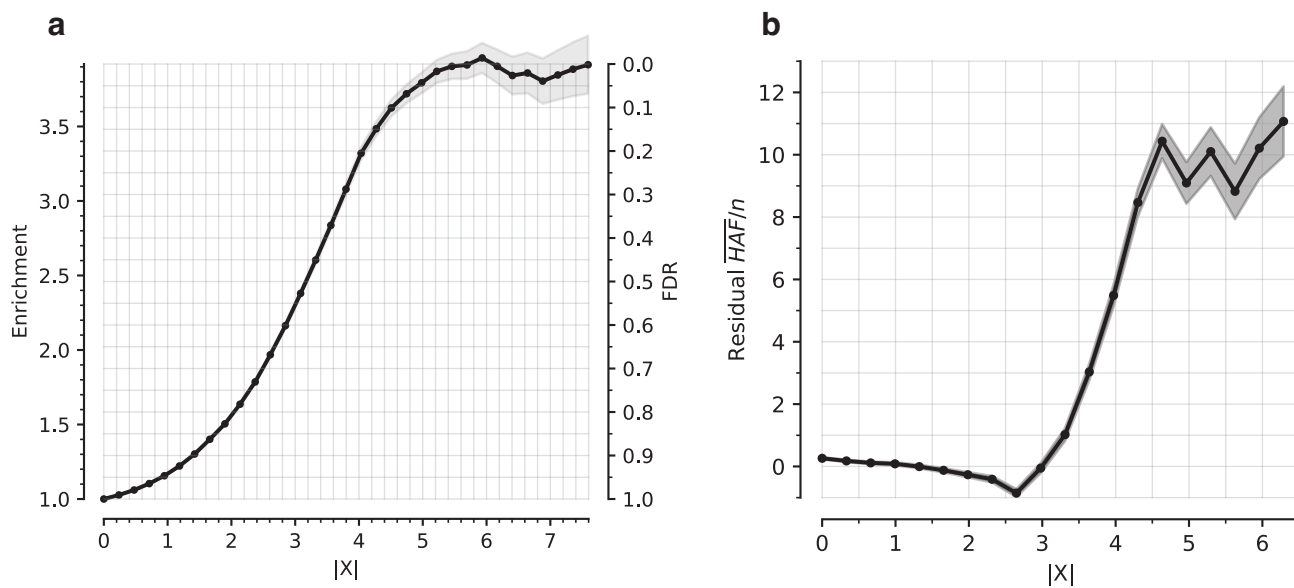
137. Krzewińska, M. *et al.* Genomic and Strontium Isotope Variation Reveal Immigration Patterns in a Viking Age Town. *Curr. Biol.* **28**, 2730–2738.e10 (2018).
138. Skoglund, P. *et al.* Genomic Diversity and Admixture Differs for Stone-Age Scandinavian Foragers and Farmers. *Science* **344**, 747–750 (2014).
139. Skourtanioti, E. *et al.* Genomic History of Neolithic to Bronze Age Anatolia, Northern Levant, and Southern Caucasus. *Cell* **181**, 1158–1175.e28 (2020).
140. Lazaridis, I. *et al.* Genomic insights into the origin of farming in the ancient Near East. *Nature* **536**, 419–424 (2016).
141. Martiniano, R. *et al.* Genomic signals of migration and continuity in Britain before the Anglo-Saxons. *Nat. Commun.* **7**, 10326 (2016).
142. Villalba-Mouco, V. *et al.* Genomic transformation and social organization during the Copper Age–Bronze Age transition in southern Iberia. *Sci. Adv.* **7**, eabi7038 (2021).
143. Seguin-Orlando, A. *et al.* Heterogeneous Hunter-Gatherer and Steppe-Related Ancestries in Late Neolithic and Bell Beaker Genomes from Present-Day France. *Curr. Biol.* **31**, 1072–1083.e10 (2021).
144. Ingman, T. *et al.* Human mobility at Tell Atchana (Alalakh), Hatay, Turkey during the 2nd millennium BC: Integration of isotopic and genomic evidence. *PLOS ONE* **16**, e0241883 (2021).
145. Schiffels, S. *et al.* Iron Age and Anglo-Saxon genomes from East England reveal British migration history. *Nat. Commun.* **7**, 10408 (2016).
146. Armit, I. *et al.* Kinship practices in Early Iron Age South-east Europe: genetic and isotopic analysis of burials from the Dolge njive barrow cemetery, Dolenjska, Slovenia. *Antiquity* **97**, 403–418 (2023).
147. Mittnik, A. *et al.* Kinship-based social inequality in Bronze Age Europe. *Science* **366**, 731–734 (2019).
148. Patterson, N. *et al.* Large-scale migration into Britain during the Middle to Late Bronze Age. *Nature* **601**, 588–594 (2022).
149. Feldman, M. *et al.* Late Pleistocene human genome suggests a local origin for the first farmers of central Anatolia. *Nat. Commun.* **10**, 1218 (2019).
150. Burger, J. *et al.* Low Prevalence of Lactase Persistence in Bronze Age Europe Indicates Ongoing Strong Selection over the Last 3,000 Years. *Curr. Biol.* **30**, 4307–4315.e13 (2020).
151. Sánchez-Quinto, F. *et al.* Megalithic tombs in western and northern Neolithic Europe were linked to a kindred society. *Proc. Natl. Acad. Sci.* **116**, 9469–9474 (2019).
152. Cassidy, L. M. *et al.* Neolithic and Bronze Age migration to Ireland and establishment of the insular Atlantic genome. *Proc. Natl. Acad. Sci.* **113**, 368–373 (2016).
153. Fischer, C.-E. *et al.* Origin and mobility of Iron Age Gaulish groups in present-day France revealed through archaeogenomics. *iScience* **25**, 104094 (2022).
154. Posth, C. *et al.* Palaeogenomics of Upper Palaeolithic to Neolithic European hunter-gatherers. *Nature* **615**, 117–126 (2023).
155. González-Fortes, G. *et al.* Paleogenomic Evidence for Multi-generational Mixing between Neolithic Farmers and Mesolithic Hunter-Gatherers in the Lower Danube Basin. *Curr. Biol.* **27**, 1801–1810.e10 (2017).
156. Lipson, M. *et al.* Parallel palaeogenomic transects reveal complex genetic history of early European farmers. *Nature* **551**, 368–372 (2017).
157. Childebayeva, A. *et al.* Population Genetics and Signatures of Selection in Early Neolithic European Farmers. *Mol. Biol. Evol.* **39**, msac108 (2022).
158. Veeramah, K. R. *et al.* Population genomic analysis of elongated skulls reveals extensive female-biased immigration in Early Medieval Bavaria. *Proc. Natl. Acad. Sci.* **115**, 3494–3499 (2018).

159. Allentoft, M. E. *et al.* Population genomics of Bronze Age Eurasia. *Nature* **522**, 167–172 (2015).
160. Günther, T. *et al.* Population genomics of Mesolithic Scandinavia: Investigating early postglacial migration routes and high-latitude adaptation. *PLOS Biol.* **16**, e2003703 (2018).
161. Margaryan, A. *et al.* Population genomics of the Viking world. *Nature* **585**, 390–396 (2020).
162. Zeng, T. C. *et al.* Postglacial genomes from foragers across Northern Eurasia reveal prehistoric mobility associated with the spread of the Uralic and Yeniseian languages. Preprint at <https://doi.org/10.1101/2023.10.01.560332> (2023).
163. Freilich, S. *et al.* Reconstructing genetic histories and social organisation in Neolithic and Bronze Age Croatia. *Sci. Rep.* **11**, 16729 (2021).
164. Järve, M. *et al.* Shifts in the Genetic Landscape of the Western Eurasian Steppe Associated with the Beginning and End of the Scythian Dominance. *Curr. Biol.* **29**, 2430-2441.e10 (2019).
165. Gelabert, P. *et al.* Social and genetic diversity among the first farmers of Central Europe. Preprint at <https://doi.org/10.1101/2023.07.07.548126> (2023).
166. Koptekin, D. *et al.* Spatial and temporal heterogeneity in human mobility patterns in Holocene Southwest Asia and the East Mediterranean. *Curr. Biol.* **33**, 41-57.e15 (2023).
167. Antonio, M. L. *et al.* Stable population structure in Europe since the Iron Age, despite high mobility. *eLife* **13**, e79714 (2024).
168. Villalba-Mouco, V. *et al.* Survival of Late Pleistocene Hunter-Gatherer Ancestry in the Iberian Peninsula. *Curr. Biol.* **29**, 1169-1177.e7 (2019).
169. Gretzinger, J. *et al.* The Anglo-Saxon migration and the formation of the early English gene pool. *Nature* **610**, 112–119 (2022).
170. Saag, L. *et al.* The Arrival of Siberian Ancestry Connecting the Eastern Baltic to Uralic Speakers further East. *Curr. Biol.* **29**, 1701-1711.e16 (2019).
171. Olalde, I. *et al.* The Beaker phenomenon and the genomic transformation of northwest Europe. *Nature* **555**, 190–196 (2018).
172. Kılınç, G. M. *et al.* The Demographic Development of the First Farmers in Anatolia. *Curr. Biol.* **26**, 2659–2666 (2016).
173. Reitsema, L. J. *et al.* The diverse genetic origins of a Classical period Greek army. *Proc. Natl. Acad. Sci.* **119**, e2205272119 (2022).
174. De Barros Damgaard, P. *et al.* The first horse herders and the impact of early Bronze Age steppe expansions into Asia. *Science* **360**, eaar7711 (2018).
175. Narasimhan, V. M. *et al.* The formation of human populations in South and Central Asia. *Science* **365**, eaat7487 (2019).
176. Fu, Q. *et al.* The genetic history of Ice Age Europe. *Nature* **534**, 200–205 (2016).
177. Rodríguez-Varela, R. *et al.* The genetic history of Scandinavia from the Roman Iron Age to the present. *Cell* **186**, 32-46.e19 (2023).
178. Lazaridis, I. *et al.* The genetic history of the Southern Arc: A bridge between West Asia and Europe. *Science* **377**, eabm4247 (2022).
179. Aneli, S. *et al.* The Genetic Origin of Daunians and the Pan-Mediterranean Southern Italian Iron Age Context. *Mol. Biol. Evol.* **39**, msac014 (2022).
180. Maróti, Z. *et al.* The genetic origin of Huns, Avars, and conquering Hungarians. *Curr. Biol.* **32**, 2858-2870.e7 (2022).
181. Lazaridis, I. *et al.* The Genetic Origin of the Indo-Europeans. Preprint at <https://doi.org/10.1101/2024.04.17.589597> (2024).
182. Mittnik, A. *et al.* The genetic prehistory of the Baltic Sea region. *Nat. Commun.* **9**, 442 (2018).

183. Malmström, H. *et al.* The genomic ancestry of the Scandinavian Battle Axe Culture people and their relation to the broader Corded Ware horizon. *Proc. R. Soc. B Biol. Sci.* **286**, 20191528 (2019).
184. Mathieson, I. *et al.* The genomic history of southeastern Europe. *Nature* **555**, 197–203 (2018).
185. Clemente, F. *et al.* The genomic history of the Aegean palatial civilizations. *Cell* **184**, 2565–2586.e21 (2021).
186. Olalde, I. *et al.* The genomic history of the Iberian Peninsula over the past 8000 years. *Science* **363**, 1230–1234 (2019).
187. Marchi, N. *et al.* The genomic origins of the world's first farmers. *Cell* **185**, 1842–1859.e18 (2022).
188. Coutinho, A. *et al.* The Neolithic Pitted Ware culture foragers were culturally but not genetically influenced by the Battle Axe culture herders. *Am. J. Phys. Anthropol.* **172**, 638–649 (2020).
189. Jones, E. R. *et al.* The Neolithic Transition in the Baltic Was Not Driven by Admixture with Early European Farmers. *Curr. Biol.* **27**, 576–582 (2017).
190. Posth, C. *et al.* The origin and legacy of the Etruscans through a 2000-year archeogenomic time transect. *Sci. Adv.* **7**, eabi7673 (2021).
191. Martiniano, R. *et al.* The population genomics of archaeological transition in west Iberia: Investigation of ancient substructure using imputation and haplotype-based methods. *PLOS Genet.* **13**, e1006852 (2017).
192. Fernandes, D. M. *et al.* The spread of steppe and Iranian-related ancestry in the islands of the western Mediterranean. *Nat. Ecol. Evol.* **4**, 334–345 (2020).
193. Rohland, N. *et al.* Three assays for in-solution enrichment of ancient human DNA at more than a million SNPs. *Genome Res.* **32**, 2068–2078 (2022).
194. Amorim, C. E. G. *et al.* Understanding 6th-century barbarian social organization and migration through paleogenomics. *Nat. Commun.* **9**, 3547 (2018).
195. Schroeder, H. *et al.* Unraveling ancestry, kinship, and violence in a Late Neolithic mass grave. *Proc. Natl. Acad. Sci.* **116**, 10705–10710 (2019).
196. Jones, E. R. *et al.* Upper Palaeolithic genomes reveal deep roots of modern Eurasians. *Nat. Commun.* **6**, 8912 (2015).
197. Meyer, M. *et al.* A High-Coverage Genome Sequence from an Archaic Denisovan Individual. *Science* **338**, 222–226 (2012).
198. Raghavan, M. *et al.* Genomic evidence for the Pleistocene and recent population history of Native Americans. *Science* **349**, aab3884 (2015).
199. Prüfer, K. *et al.* The complete genome sequence of a Neanderthal from the Altai Mountains. *Nature* **505**, 43–49 (2014).
200. Mallick, S. *et al.* The Simons Genome Diversity Project: 300 genomes from 142 diverse populations. *Nature* **538**, 201–206 (2016).
201. Raghavan, M. *et al.* Upper Palaeolithic Siberian genome reveals dual ancestry of Native Americans. *Nature* **505**, 87–91 (2014).
202. Dabney, J. *et al.* Complete mitochondrial genome sequence of a Middle Pleistocene cave bear reconstructed from ultrashort DNA fragments. *Proc. Natl. Acad. Sci.* **110**, 15758–15763 (2013).
203. Korlević, P. *et al.* Reducing Microbial and Human Contamination in DNA Extractions from Ancient Bones and Teeth. *BioTechniques* **59**, 87–93 (2015).
204. Rohland, N., Harney, E., Mallick, S., Nordenfelt, S. & Reich, D. Partial uracil-DNA-glycosylase treatment for screening of ancient DNA. *Philos. Trans. R. Soc. Lond. B. Biol. Sci.* **370**, 20130624 (2015).

205. Briggs, A. W. & Heyn, P. Preparation of next-generation sequencing libraries from damaged DNA. *Methods Mol. Biol. Clifton NJ* **840**, 143–154 (2012).
206. Fu, Q. *et al.* DNA analysis of an early modern human from Tianyuan Cave, China. *Proc. Natl. Acad. Sci. U. S. A.* **110**, 2223–2227 (2013).
207. Haak, W. *et al.* Massive migration from the steppe was a source for Indo-European languages in Europe. *Nature* **522**, 207–211 (2015).
208. Rohland, N., Glocke, I., Aximu-Petri, A. & Meyer, M. Extraction of highly degraded DNA from ancient bones, teeth and sediments for high-throughput sequencing. *Nat. Protoc.* **13**, 2447–2461 (2018).
209. Gansauge, M.-T., Aximu-Petri, A., Nagel, S. & Meyer, M. Manual and automated preparation of single-stranded DNA libraries for the sequencing of DNA from ancient biological remains and other sources of highly degraded DNA. *Nat. Protoc.* **15**, 2279–2300 (2020).
210. Li, H. & Durbin, R. Fast and accurate short read alignment with Burrows-Wheeler transform. *Bioinforma. Oxf. Engl.* **25**, 1754–1760 (2009).
211. Picard toolkit. *Broad Institute, GitHub repository* (2019).
212. Behar, D. M. *et al.* A “Copernican” Reassessment of the Human Mitochondrial DNA Tree from its Root. *Am. J. Hum. Genet.* **90**, 675–684 (2012).
213. 1000 Genomes Project Consortium *et al.* A global reference for human genetic variation. *Nature* **526**, 68–74 (2015).
214. Danecek, P. *et al.* Twelve years of SAMtools and BCFtools. *GigaScience* **10**, giab008 (2021).
215. Zhao, H. *et al.* CrossMap: a versatile tool for coordinate conversion between genome assemblies. *Bioinforma. Oxf. Engl.* **30**, 1006–1007 (2014).
216. Karczewski, K. J. *et al.* The mutational constraint spectrum quantified from variation in 141,456 humans. *Nature* **581**, 434–443 (2020).
217. Gazal, S. S-LDSC reference files. Zenodo <https://doi.org/10.5281/zenodo.10515792> (2024).
218. Sakaue, S. *et al.* A cross-population atlas of genetic associations for 220 human phenotypes. *Nat. Genet.* **53**, 1415–1424 (2021).
219. Chen, T.-T. *et al.* Shared genetic architectures of educational attainment in East Asian and European populations. *Nat. Hum. Behav.* **8**, 562–575 (2024).
220. Shelton, J. F. *et al.* Trans-ancestry analysis reveals genetic and nongenetic associations with COVID-19 susceptibility and severity. *Nat. Genet.* **53**, 801–808 (2021).

**Figure 1**



**c**

Category	Number of traits	Heritability enrichment (95% CI)	Z-score for selection stronger in	
			Bronze Age than Neolithic/Mesolithic	Historical period than Bronze Age
Biomarkers	9	4.03 (2.28-5.78)	2.84	0.74
Blood/immune/inflammatory	20	4.71 (2.65-6.77)	3.82	1.50
Cardio/metabolic	20	1.55 (1.09-2.01)	3.53	-0.08
Life history/reproduction	7	1.54 (1.13-1.95)	1.95	-1.06
Behavioral	13	0.96 (0.55-1.36)	-0.14	1.43
Mental/psychiatric/nervous	13	0.77 (0.23-1.31)	0.26	0.44
Other	25	1.47 (1.03-1.91)	2.98	1.31
All	107	1.87 (1.43-2.31)	6.49	2.01

**Figure 2**

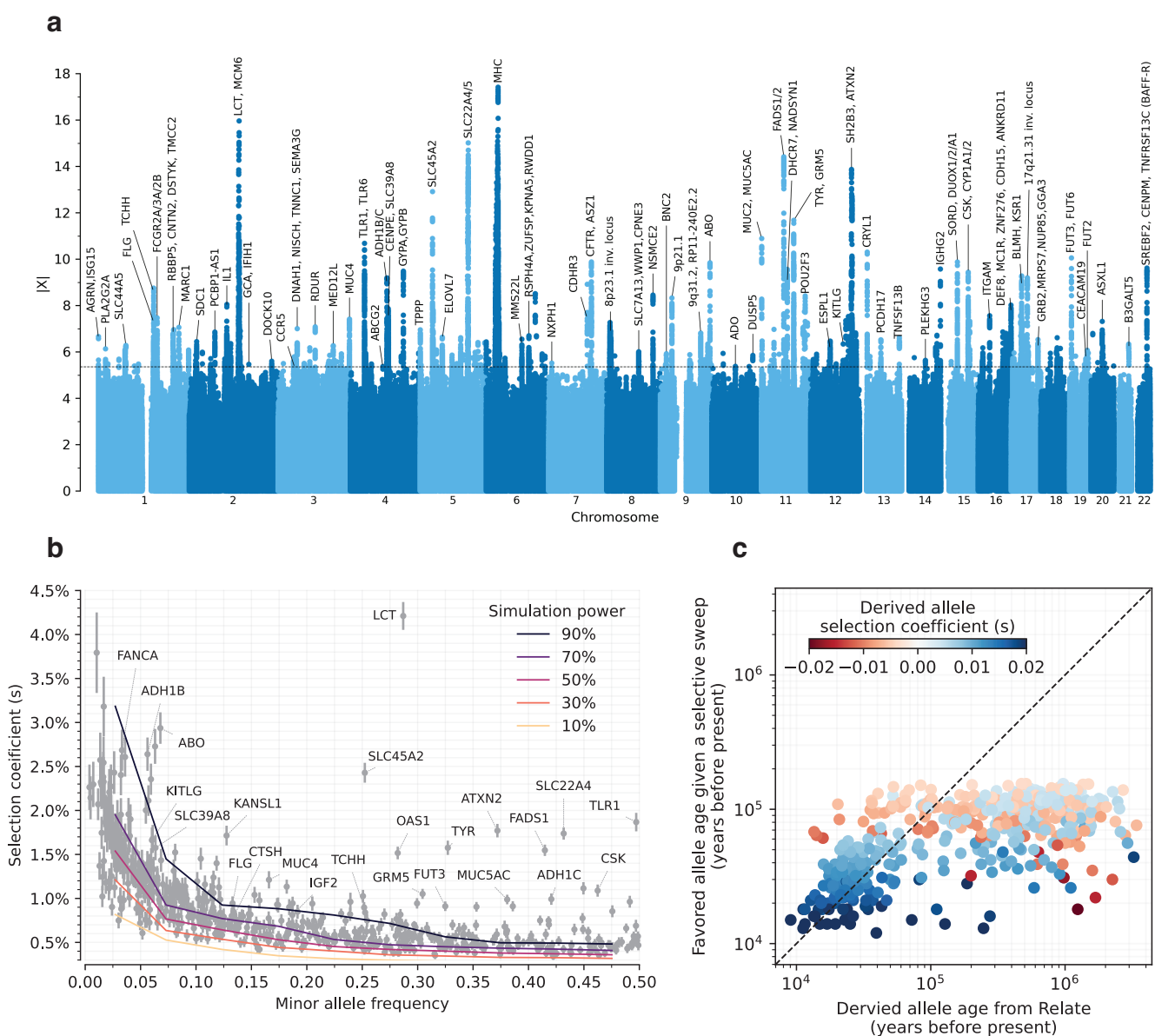


## Figure 3

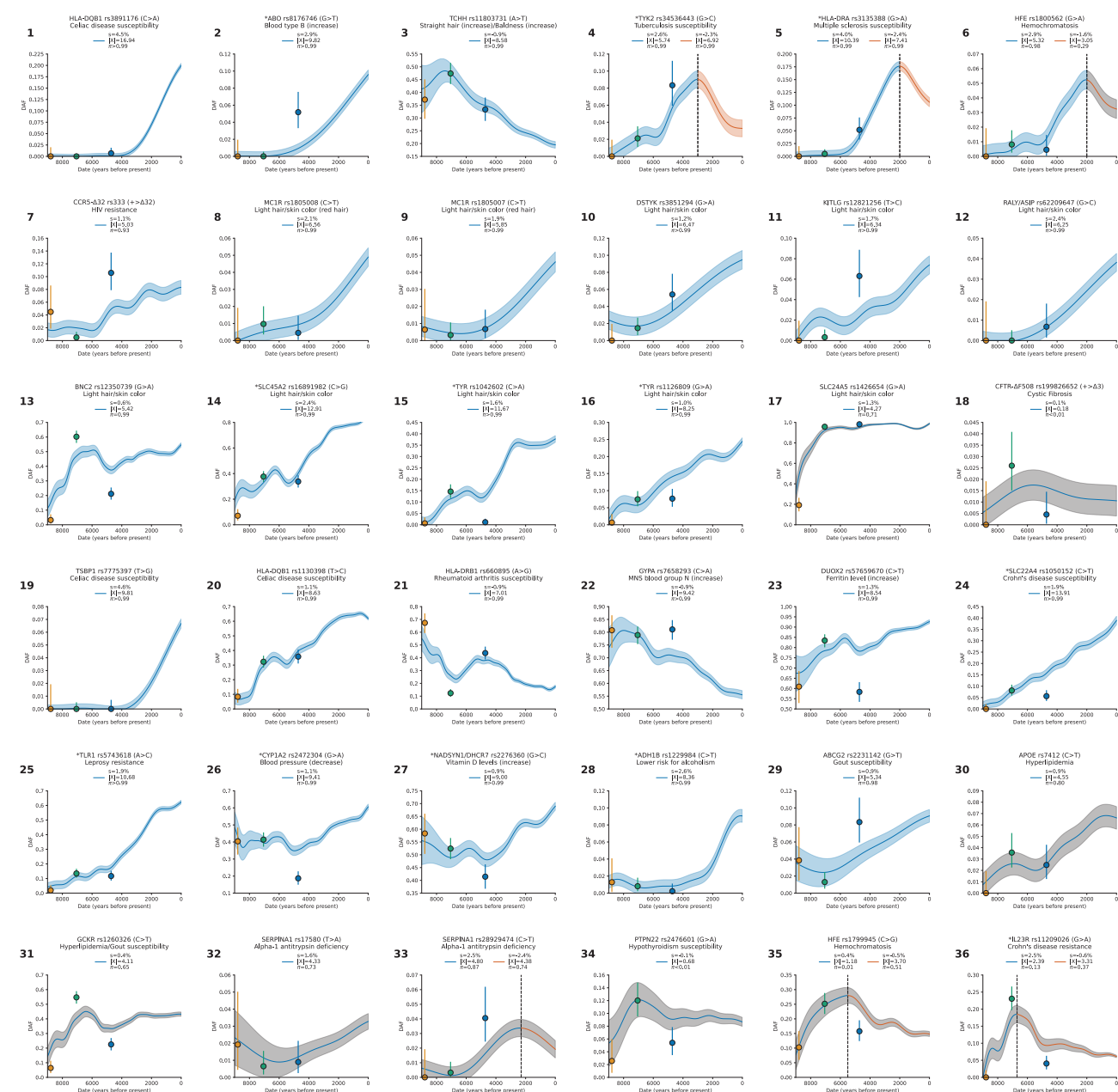
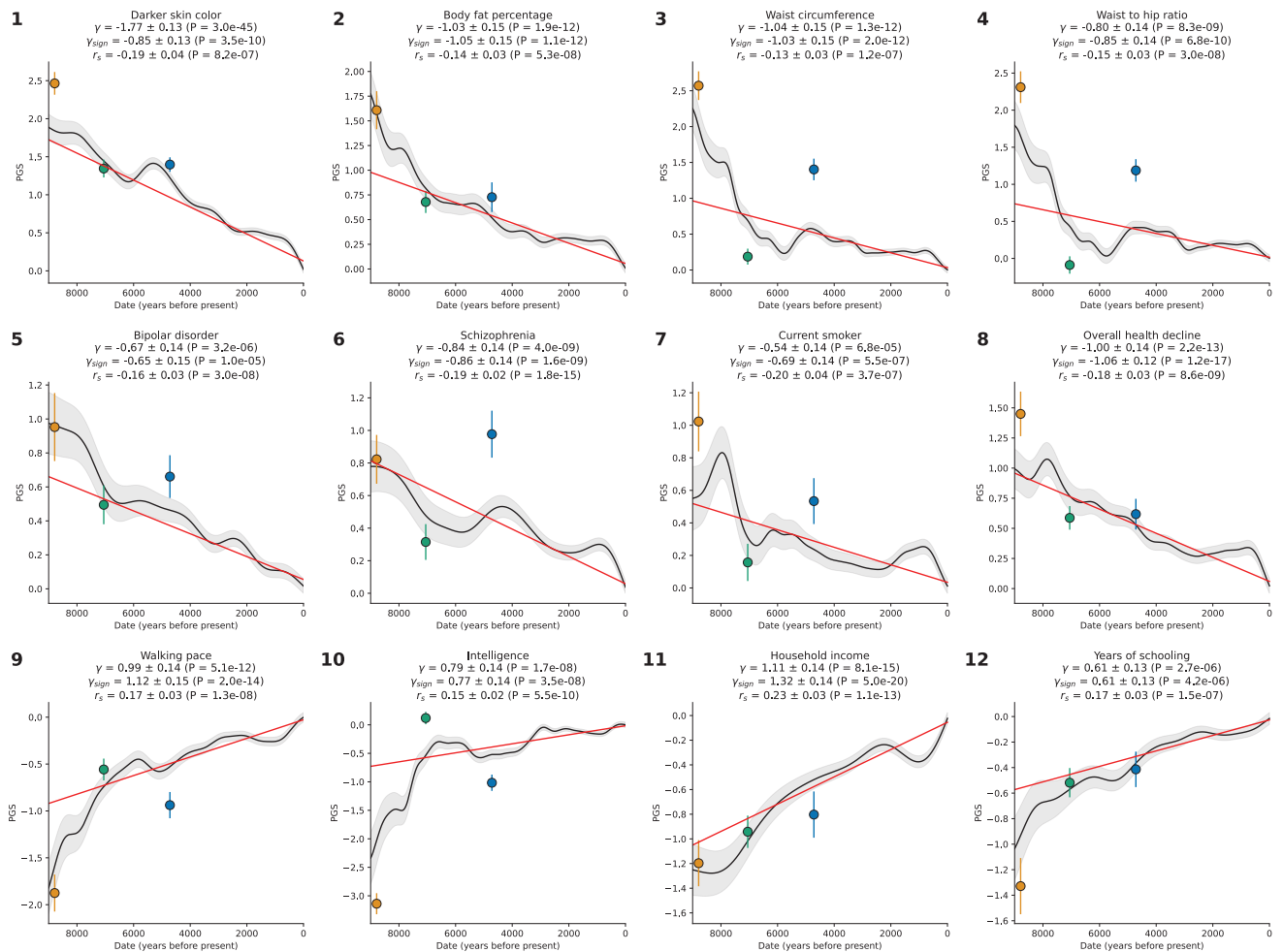
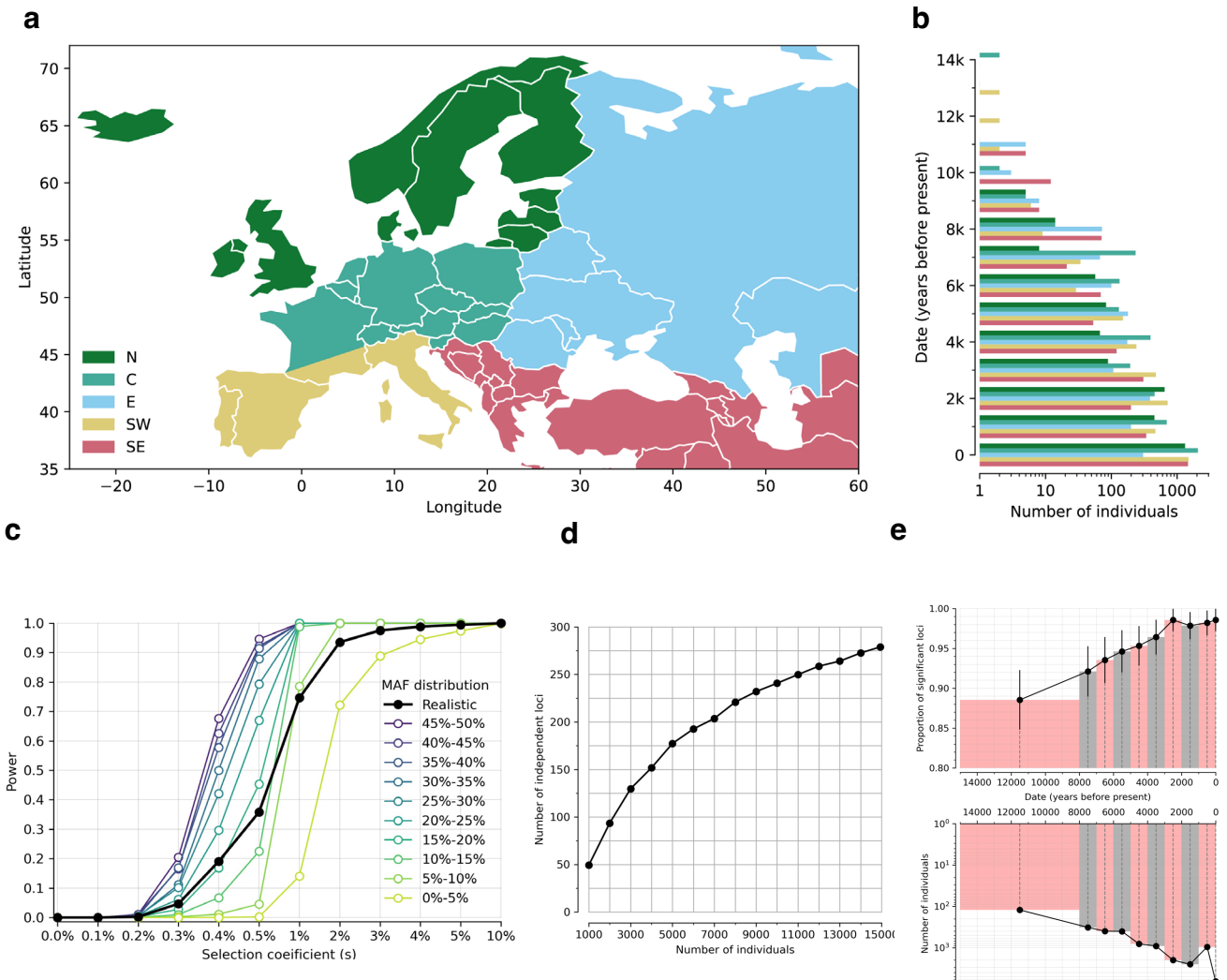


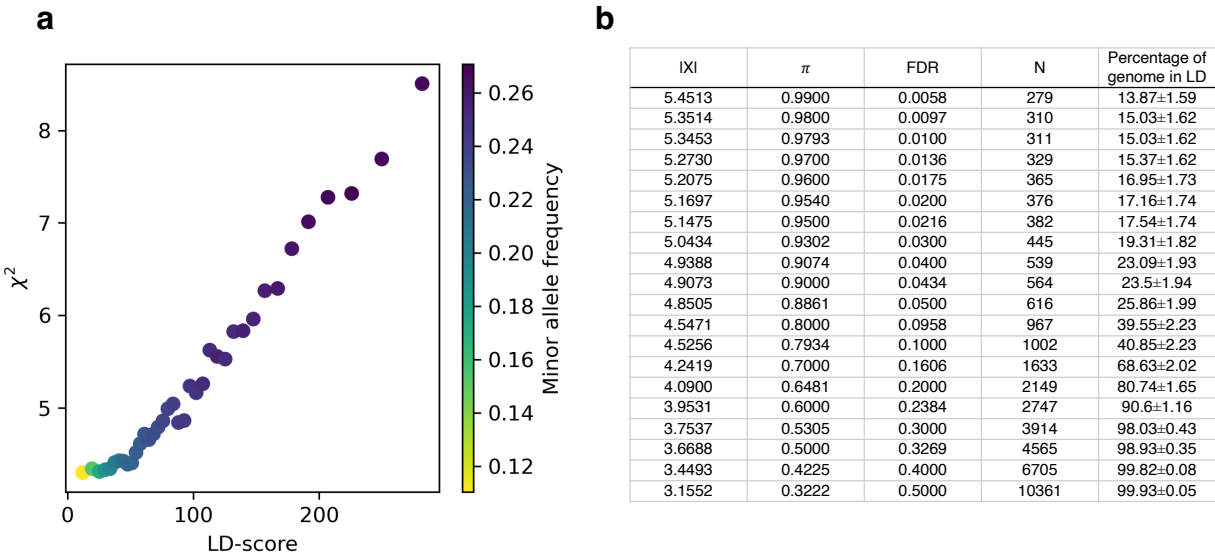
## Figure 4



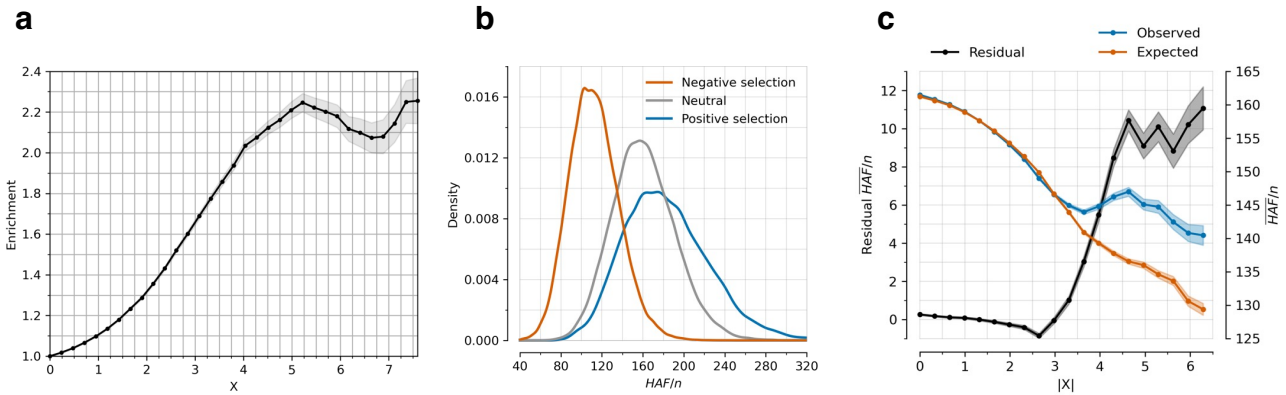
## Extended Data Figure 1



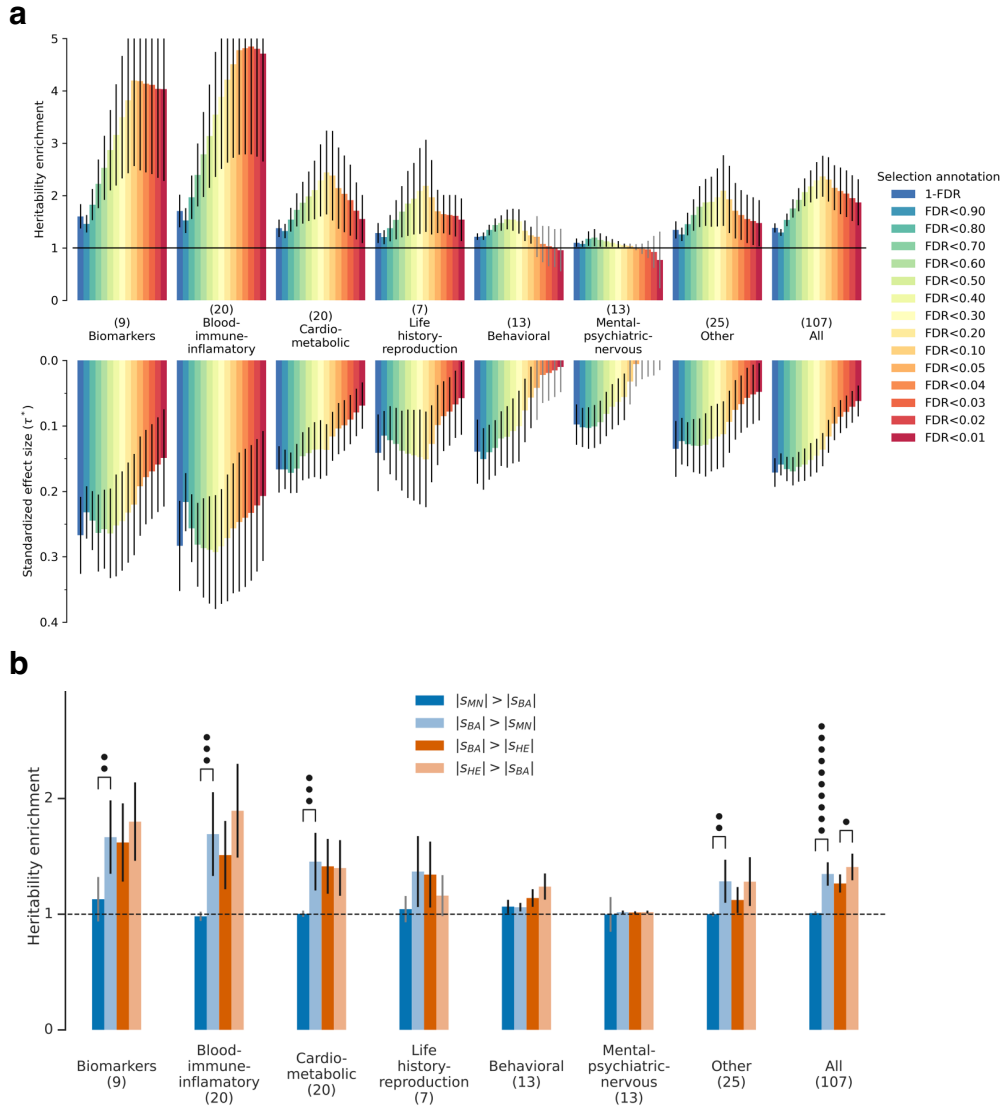
## Extended Data Figure 2



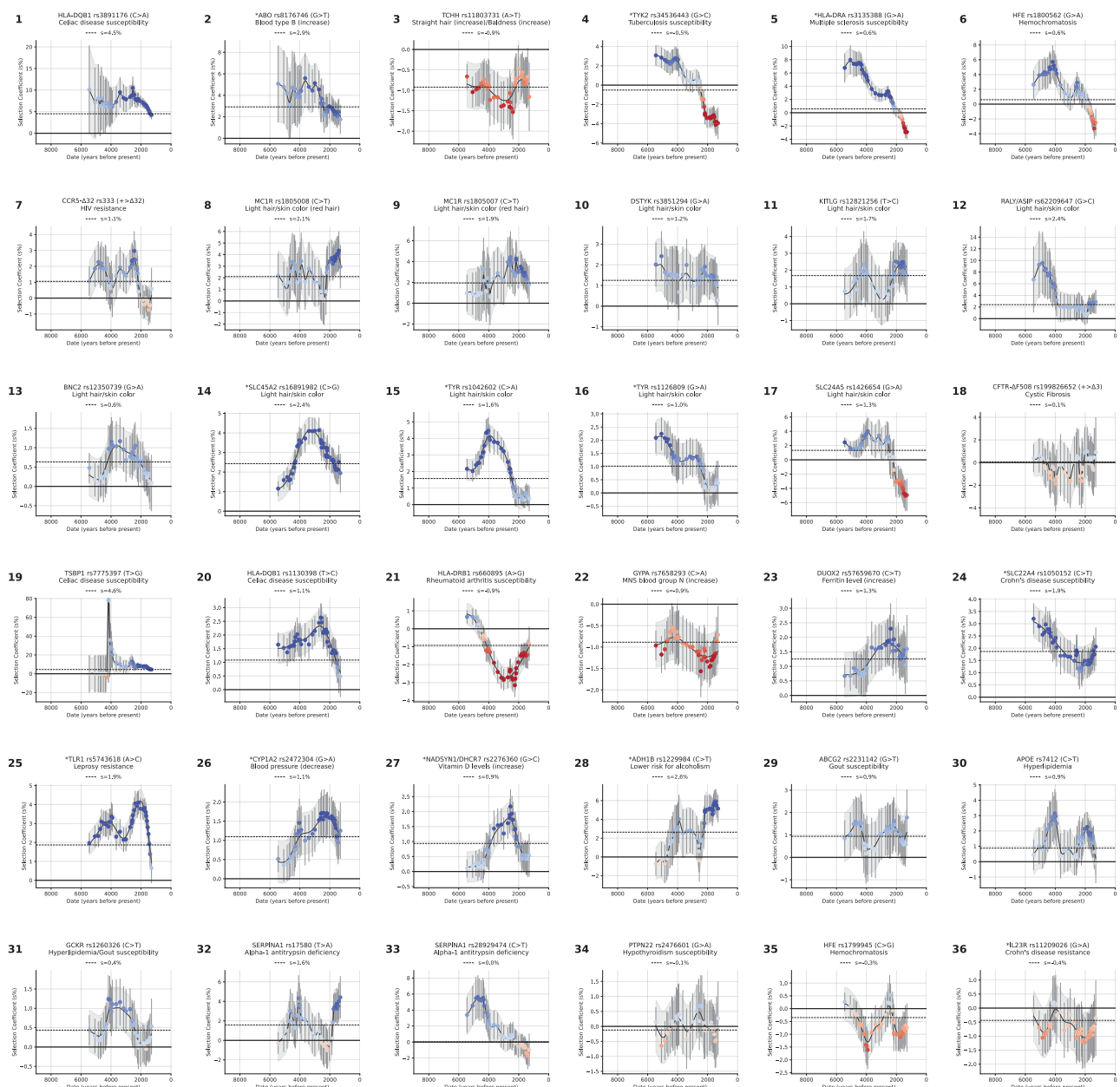
## Extended Data Figure 3



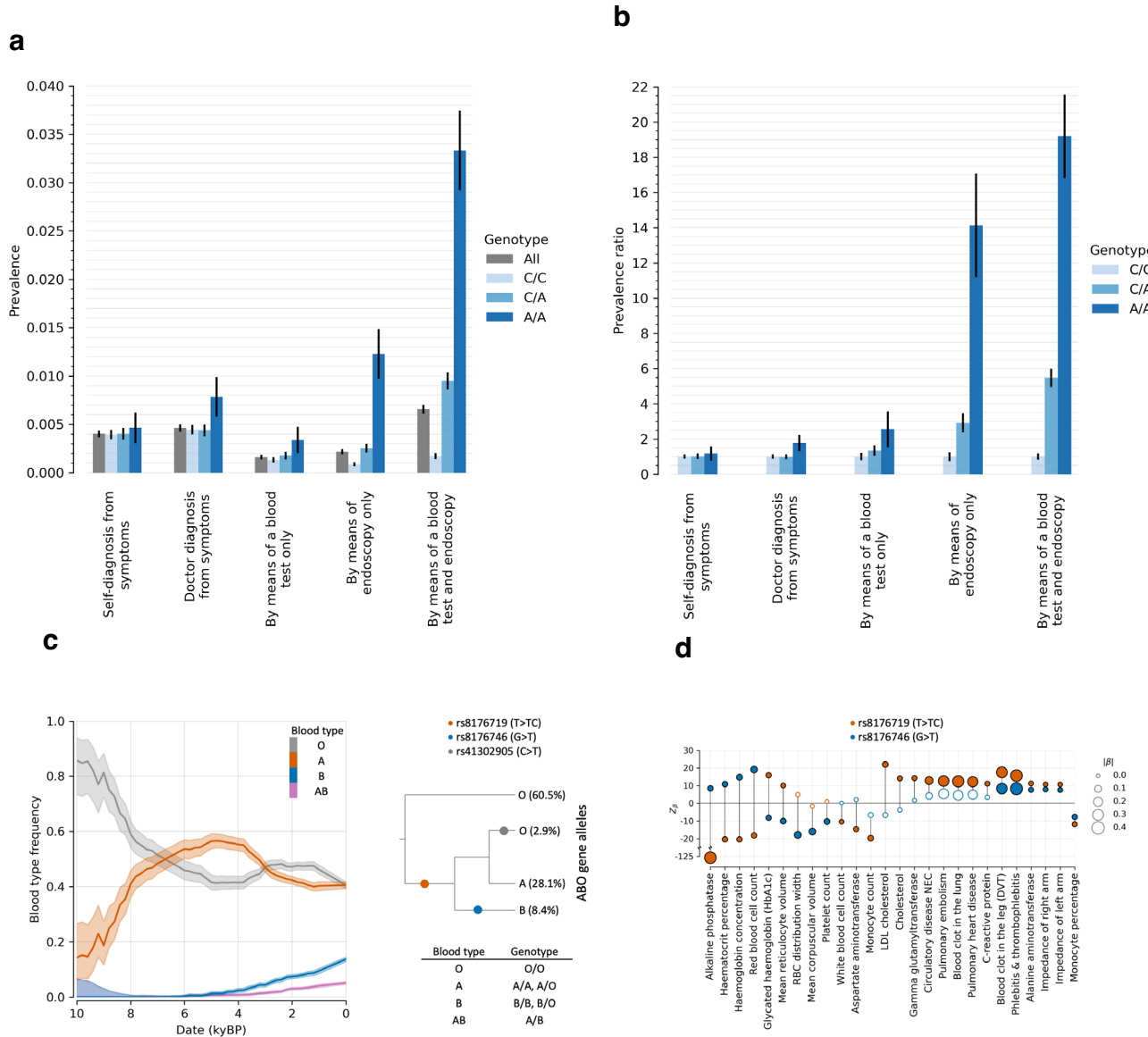
## Extended Data Figure 4



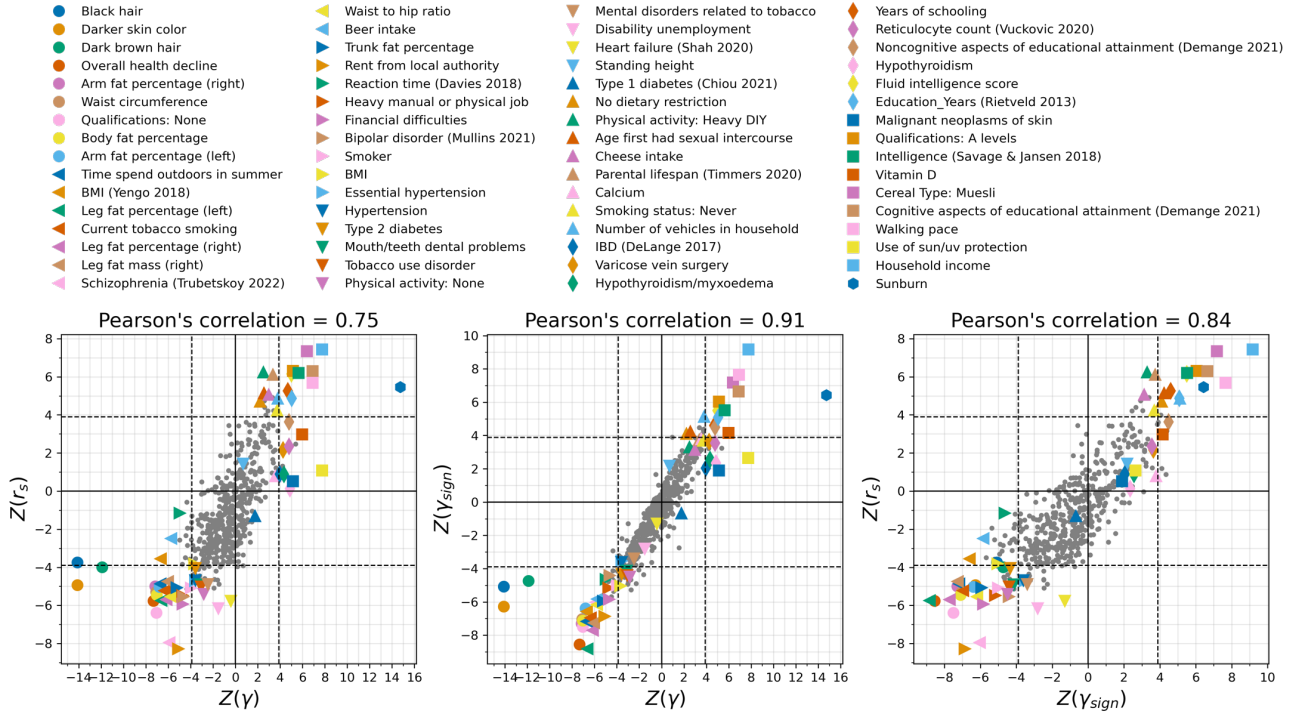
## Extended Data Figure 5



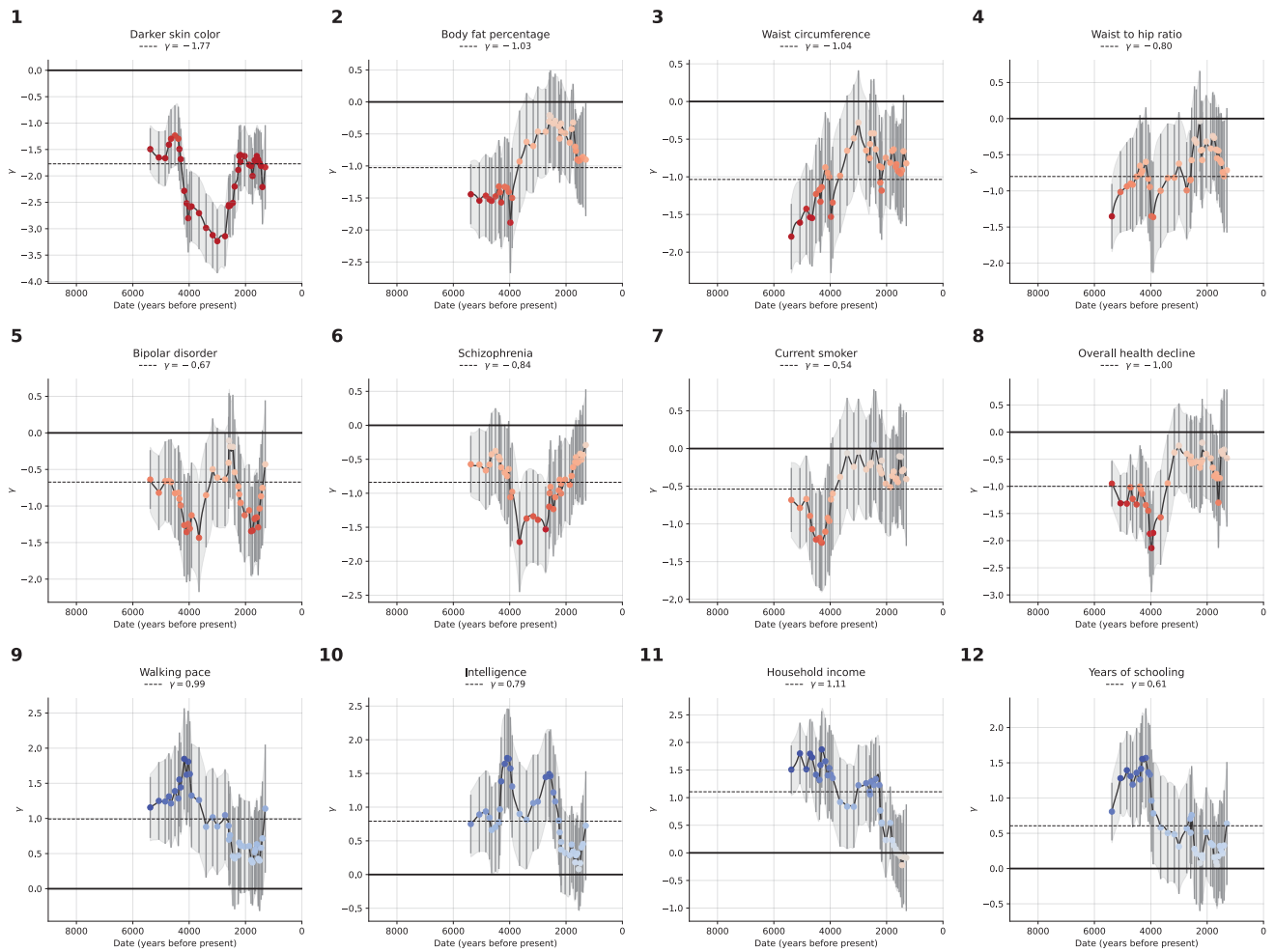
## Extended Data Figure 6



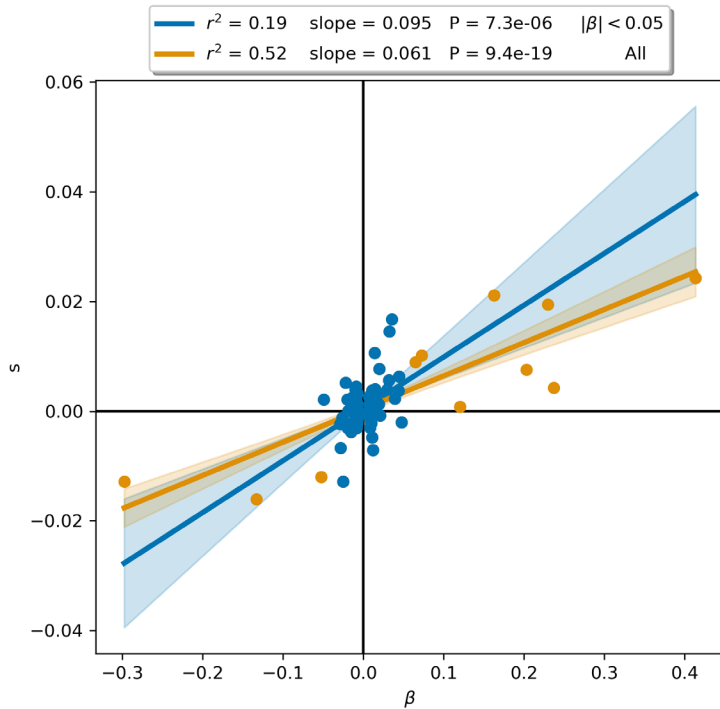
## Extended Data Figure 7



## Extended Data Figure 8



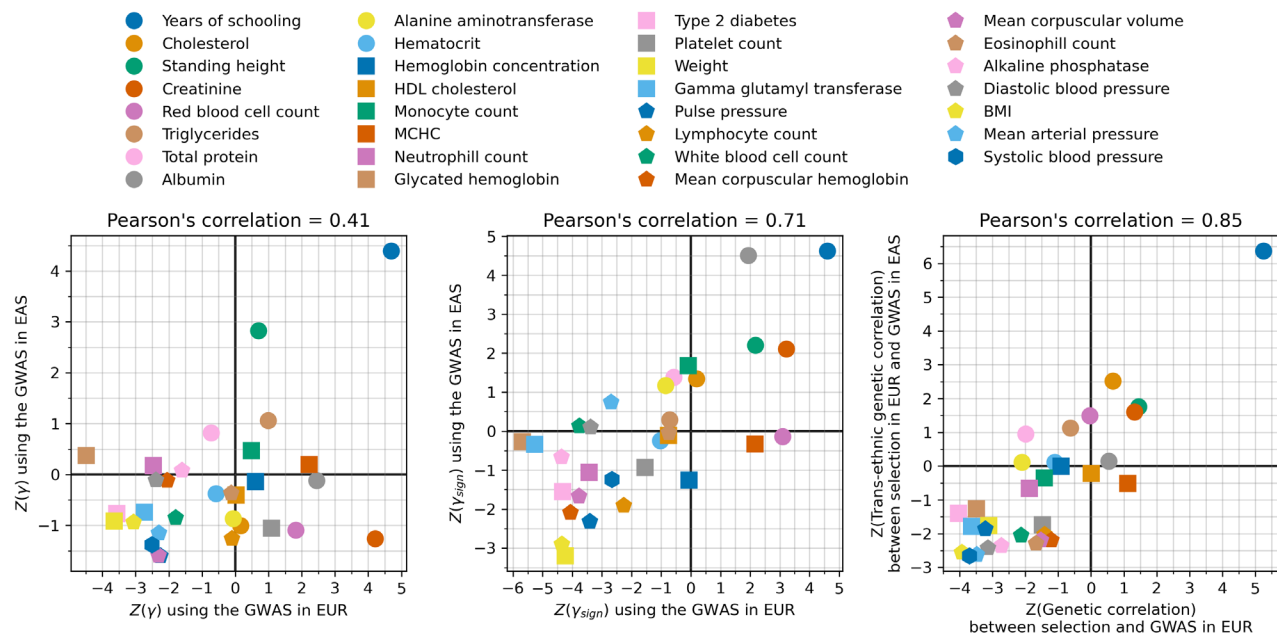
## Extended Data Figure 9



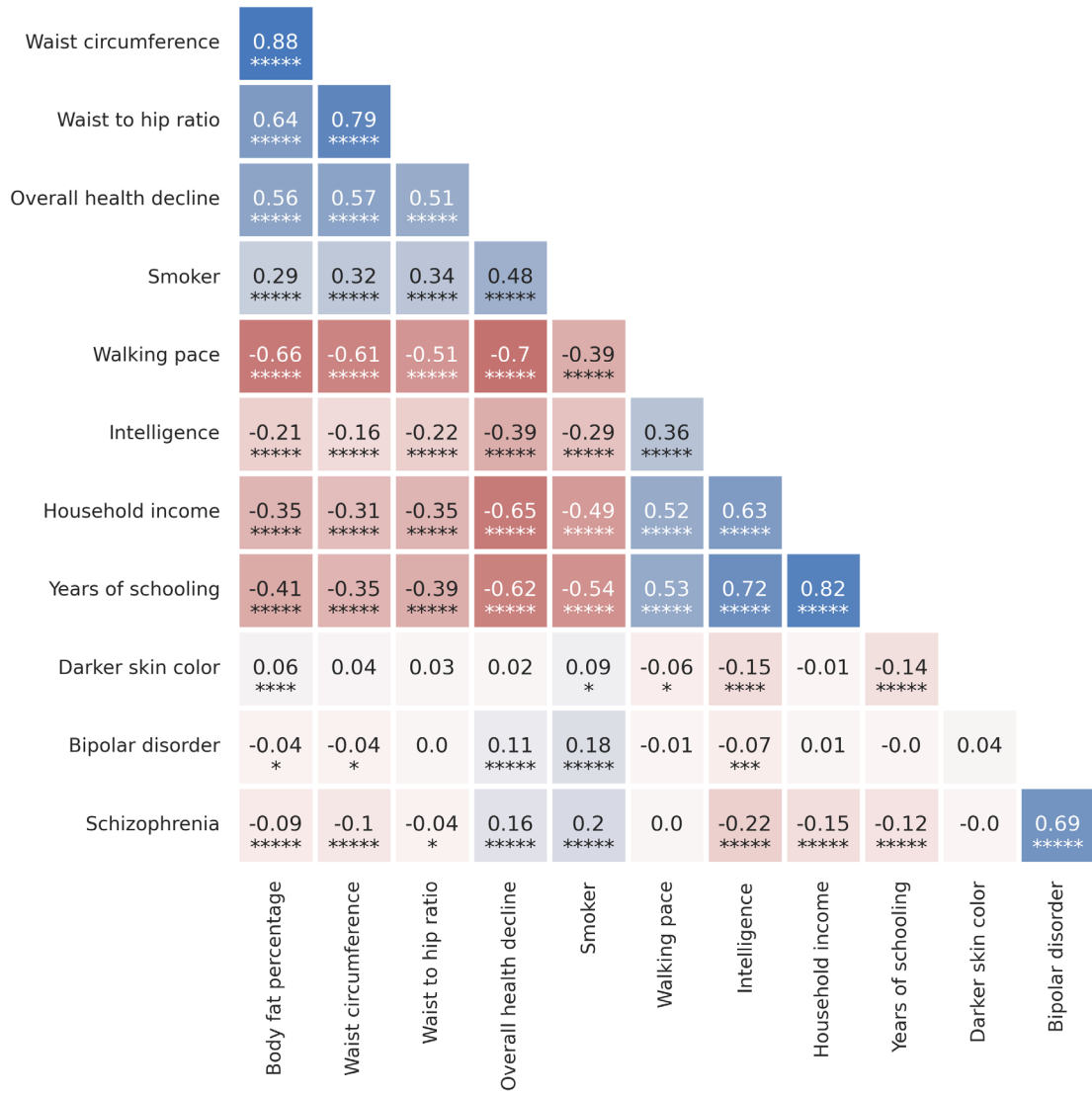
## Extended Data Figure 10



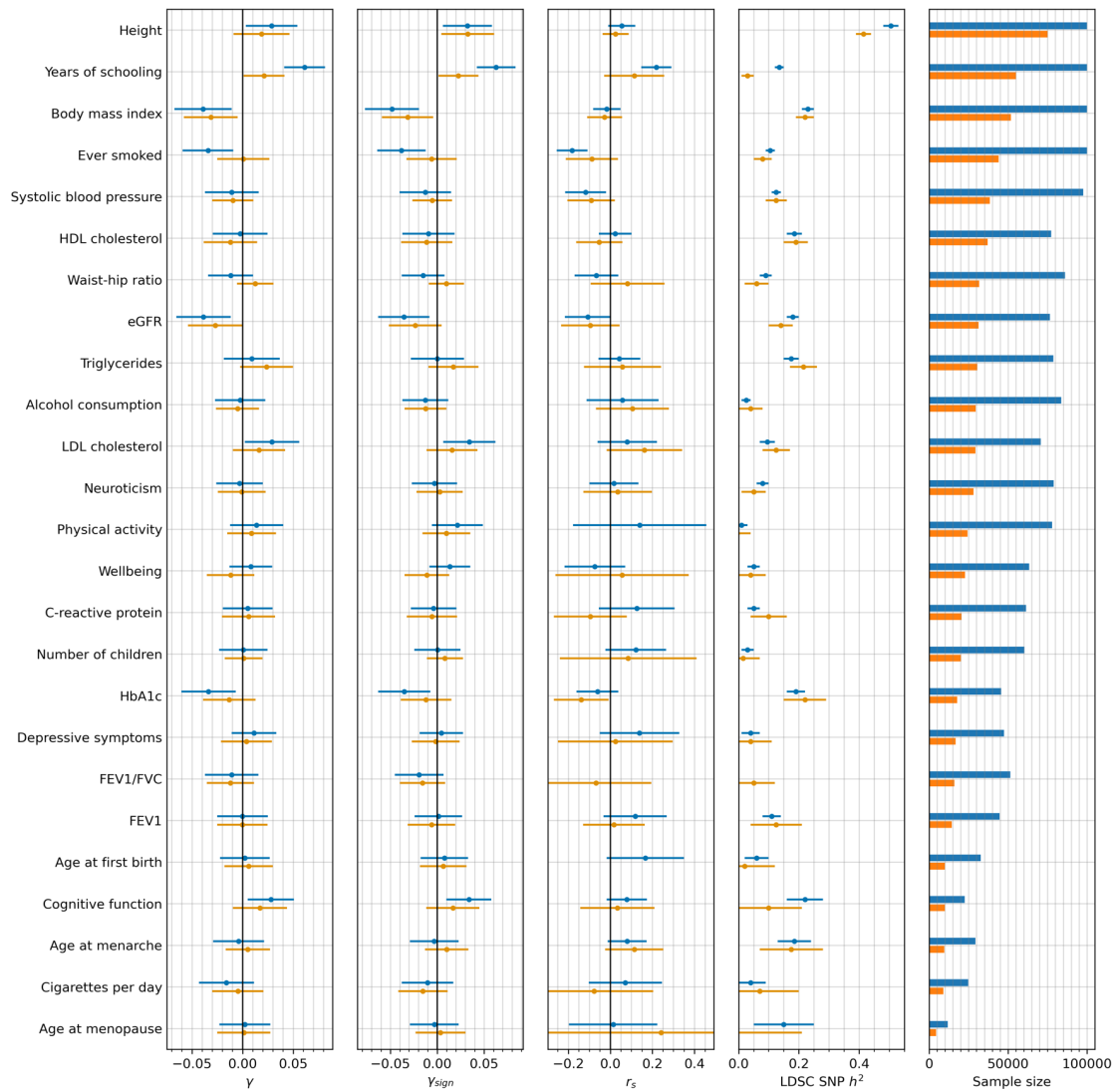
## Extended Data Figure 11



## Extended Data Figure 12



## Extended Data Figure 13



## Extended Data Figure 14

